Scaling in pinch-off of generalized Newtonian fluids

Pankaj Doshi[1], Ronald Suryo[1], Ozgur E. Yildirim[1],

Gareth H. McKinley[2] and Osman A. Basaran[1]

March 26, 2003

[1]School of Chemical Engineering, Purdue University, West Lafayette, IN 47907, USA

[2]Department of Mechanical Engineering, Massachusetts Institute of Technology,

Cambridge, Massachusetts 02139

Abstract

Pinch-off dynamics of slender liquid bridges of generalized Newtonian fluids without and with inertia are studied using asymptotic analysis and numerical computation. The deformation-rate-dependent rheology is described by power law and Carreau models. Because the bridges are slender, their dynamics are governed by a pair of spatially one-dimensional, nonlinear evolution equations for the bridge shape and axial velocity. A bridge of a power law fluid under creeping flow conditions exhibits self-similar dynamics

in the vicinity of the axial location where the bridge radius is a minimum. The scaling exponents that determine the variation with time remaining to breakup of the bridge radius or radial length scale, axial length scale, and axial velocity are evaluated by a combined analytical and numerical approach. Similarity solutions are obtained by collapsing numerically computed profiles of both the bridge shape and the axial velocity in the vicinity of the axial location where the bridge radius is minimum by rescaling of the transient profiles with radial and axial scalings deduced from theory. This scaling behavior is transitory and inertial effects become significant as pinch-off is approached. Thereafter, a new balance is established between viscous, capillary, and inertial forces that leads to a new self-similar regime which persists until pinch-off. The scaling exponents appropriate to this regime are also determined. Moreover, it is shown theoretically that interface shapes in the vicinity of the singularity are non-slender for values of the power law exponent below 2/3. Similarity solutions are once again obtained in the same manner as that used in the creeping flow limit. Low-viscosity bridges of Carreau fluids are known to exhibit a transition from potential flow scaling to Newtonian scaling. Here it is demonstrated that high-viscosity bridges of Carreau fluids exhibit a transition from power law scaling to Newtonian scaling. The point of transition between the latter two regimes is predicted in terms of parameters of the Carreau model.

Keywords: Drop breakup; Jet breakup; Interface rupture; Capillary pinch-off; Scaling; Self-similarity; Non-Newtonian fluids

1 Introduction

Dynamics and breakup of liquid threads and jets driven by the capillary instability have been studied for more than a century [1] due to their importance in various practical applications as ink-jet printing [2], fiber spinning [3] and filament-stretching rheometry [4]. A space-time singularity occurs when the minimum radius of a breaking thread shrinks to zero, resulting in the blow-up of the values of the interfacial curvature and axial velocity at the pinch point. Length and time scales of the motion close to pinch-off are much smaller than those of the bulk motion so that the dynamics near the singularity ought to evolve virtually independently of the initial and boundary conditions, and thus exhibit self-similarity.

Keller and Miksis [5] first proposed a scaling theory describing self-similar recoil of an inviscid liquid sheet undergoing potential flow in the aftermath of its rupture. Peregrine et al. [6] were first to suggest that the dynamics near breakup are universal, characterized by the nonlinear properties of the equations of motion. Since these early works, many authors have developed scaling theories to describe the pinch-off dynamics of Newtonian liquid threads surrounded by a dynamically inert fluid, as discussed in the next paragraph. The main objective of this paper is to advance the understanding of the pinch-off dynamics of non-Newtonian liquid threads.

Eggers [7] was first to develop an asymptotic theory of the pinch-off singularity in the situation where inertial, viscous, and capillary forces are all of the same order, a regime that

is appropriately called the inertial-viscous (IV) regime. Eggers [8] then derived the scaling functions that define the shape of the thread and the velocity field within it close to breakup as functions of the viscous length and time scales of the fluid. Before the liquid thread reaches the IV regime, however, it can pass through intermediate asymptotic regimes depending on the relative importance of inertial, viscous, and capillary forces as it thins. These regimes include (1) a potential flow (PF) regime [9] where inertial and capillary forces are important, and (2) a viscous (V) or creeping flow regime [10, 11] where only viscous and capillary forces are important. Rothert et al. [12] have carried out an experimental study which showed a transition from the V to the IV regime as breakup was approached. Similarly, a transition from the PF to the IV regime was shown both computationally and experimentally in recent papers by Notz et al. [13] and Chen et al.[14].

While the focus of most of the studies on interface rupture has been the breakup of Newtonian liquid threads, the equally important problem of the breakup of non-Newtonian liquid threads has received far less attention. In addition to the usual capillary force that drives pinch-off, non-Newtonian effects such as deformation-rate-dependent material properties, viscoelasticity, and strain-hardening, among others, are known to significantly alter the breakup dynamics [15, 16, 17, 18]. Experiments have shown that the presence of even small amounts of polymer can delay or completely suppress breakup [15]. A recent experimental study on pinch-off of a water drop with minute amounts of polymer has revealed that after a

brief period of self-similar dynamics that are unchanged from those observed with a drop of pure solvent, an abrupt transition occurs leading to an exponential thinning of the neck [16]. Experiments such as these have motivated theoretical analyses on the pinch-off dynamics of slender viscoelastic jets. In a series of papers [19, 20, 21], Renardy has studied the self-similar breakup of jets of viscoelastic fluids whose rheologies are described by various constitutive models. As pointed out by Chang et al. [22], since these analyses omit effects of inertia and focus only on slender filaments, they have been unable to capture important pre-breakup phenomena like iterated stretching and bead formation. Chang et al. [22] have studied the iterated stretching dynamics of FENE and Oldroyd-B jets by solving a set of one dimensional (1-D) slender-jet equations by numerical simulation and asymptotic analysis. These authors have shown that the universal stress scaling during self-similar pinch-off of a viscoelastic jet is quite distinct from that of a Newtonian jet, even though the radial and axial scalings are identical in the two situations. More recently, Renardy and Losh have studied the existence of similarity solutions for the surface tension driven breakup of a jet of a Giesekus fluid with inertia [23].

There have been yet fewer studies of the pinch-off dynamics of fluids with deformation-rate-dependent material properties. Renardy [20, 21] has demonstrated the existence of self-similar solutions for pinching of a thread of a power law fluid undergoing creeping flow. He used a Lagrangian formulation to derive a force balance governing the dynamics. He then

reduced this balance by a similarity ansatz with two scaling exponents. Renardy determined the value of one of the exponents by a similarity transformation but left the value of the other exponent undetermined. He also showed that the behavior of a power law fluid is qualitatively similar to that of a Newtonian fluid [11]. However, as Eggers [7] has demonstrated for the case of Newtonian fluids, inertia becomes important during the final stage of breakup of a thread and a transition occurs from viscous-capillary scaling to inertial-viscous-capillary scaling. A similar transition should be even more pronounced for deformation-rate-thinning fluids and therefore inertia should be included in the analysis of pinch-off dynamics of such fluids.

The presence of inertia in the equations of motion renders the slender-jet analysis more difficult. Recently, Yildirim and Basaran (referred to herein as YB) [17] computationally studied the dynamics of stretching liquid bridges of fluids described by the Carreau model. The deformation-rate-dependent effects in a Carreau fluid are captured by a non-Newtonian viscosity model given by [24]

$$\tilde{\mu} = \tilde{\mu}_o(1-\beta)[1+(\tilde{\alpha}\tilde{\dot{\gamma}})^2]^{((n-1)/2)} + \tilde{\mu}_o\beta \tag{1}$$

where $\tilde{\mu}$ is the apparent viscosity and $\tilde{\dot{\gamma}}^2$ is the second invariant of the rate of deformation tensor. In eq. (1), $\tilde{\mu}_o$ is the zero-shear-rate viscosity, $\tilde{\alpha}^{-1}$ is a characteristic shear rate, $\beta\tilde{\mu}_o$, where $0 \leq \beta \leq 1$, is the viscosity in the limit of infinite deformation rate, and $n \leq 1$ is a power law exponent. Section 2 provides a detailed description of eq. (1). It is noteworthy that

eq. (1) predicts the same rate-dependence of the fluid viscosity in any mode of deformation. The flow in a thinning thread is, of course, predominantly a transient, uniaxial extensional flow. However, for succinctness the fluid will henceforward be referred to simply as *shear-thinning* rather than by the more cumbersome descriptor "extension-rate-thinning." Other generalized Newtonian fluid models have been proposed which show different behavior in planar shear flow and uniaxial extension (see, for example, the work of Debbaut and Crochet [25]). However, analysis of these models is beyond the scope of the present paper.

Figure 1 shows the variation of the dimensionless viscosity $\mu \equiv \tilde{\mu}/\tilde{\mu}_o$ as predicted by eq. (1) with the dimensionless deformation rate $\dot{\gamma} \equiv \tilde{\alpha}\tilde{\dot{\gamma}}$ when $n = 0.7$ for three different values of β. In all three cases, the dimensionless viscosity shows the well known transition from an initial Newtonian response to a power law response and it eventually approaches a second Newtonian plateau corresponding to the infinite-shear-rate viscosity β. Figure 1 shows that the range of the power law region strongly depends on the value of β. The results reported by YB included comparison of breakup length, location, and time for liquid bridges of Carreau fluids with corresponding results for Newtonian fluids. YB also reported results on the scaling with time remaining to breakup of the minimum radius of bridges of low viscosity Carreau and Newtonian fluids. They showed that for bridges of both fluids, the minimum radius initially followed PF scaling theory and later transitioned to IV scaling. Through this limited exploration of the parameter space, the only difference that YB identified between

the two cases was a delayed transition from PF to IV scaling for a Carreau fluid compared to a Newtonian fluid owing to the former fluid's shear-thinning nature. Therefore, the main aim of this paper is to carry out a much more detailed analytical and numerical study of the pinch-off of shear-thinning fluids than has been carried out to date in order to determine completely the scaling behavior of a power law fluid without and with inertia, the transition between such regimes, and the transition from a power law to a final Newtonian regime for a Carreau fluid.

The paper is organized as follows. Section 2 presents the mathematical formulation of the problem starting with the two-dimensional system of equations governing the dynamics of a thinning filament. Section 2 then presents the Carreau constitutive model that is used to describe the shear-thinning behavior of the non-Newtonian fluid and discusses two limiting forms of this model. Section 2 also outlines a system of 1-D slender-jet equations for a shear-thinning fluid that is analogous to the system of equations obtained by Bechtel et al. [26] for viscoelastic fluids, and by Eggers [7, 8], Eggers and Dupont [27], and Papageorgiou [10, 11] for Newtonian fluids. Section 3 summarizes the numerical method and algorithm used to solve the system of 1-D evolution equations. Section 4 presents self-similar solutions describing the pinch-off of a power law fluid without and with inertia. Section 5 presents a number of computational results obtained with the numerical algorithm and also compares predictions of the asymptotic analyses of section 4 with predictions made with the numerical

algorithm. For the case of a power law fluid without inertia, the exponent left undetermined by Renardy [20] is also evaluated. Section 6 makes concluding remarks and suggests possible avenues for future research.

2 Mathematical Formulation

The system under study is an axisymmetric bridge of an isothermal incompressible liquid with density ρ that is held captive between two circular discs of radii R, as shown in fig. 2. The bridge is surrounded by an ambient gas that is taken to be dynamically inactive. The liquid-gas interface separating the bridge from the ambient gas has constant surface tension σ. In what follows, variables that have a tilde over them, $\tilde{()}$, are considered to be dimensional while the dimensionless counterparts of the same variables will be denoted without a tilde, $()$. The characteristic scales used for non-dimensionalization are the disc radius R for length, the zero-shear-rate viscosity $\tilde{\mu}_o$ of the bridge liquid for the deformation-rate-dependent viscosity function, and the capillary time $t_c \equiv \sqrt{\rho R^3/\sigma}$ for time. The characteristic scale for velocity is not independent but is given by $U_c \equiv R/t_c$. The isothermal, incompressible flow of liquid in the bridge is governed by Cauchy's equation of motion and the continuity equation

$$\frac{D\mathbf{v}}{Dt} = Oh\,\nabla\cdot\mathbf{T} - G\mathbf{e_z} \tag{2}$$

$$\nabla \cdot \mathbf{v} = \mathbf{0} \tag{3}$$

Here, $\mathbf{v}$ is the dimensionless fluid velocity, t is the dimensionless time, $\mathbf{e_z}$ is a unit vector that is antiparallel to gravity, $Oh \equiv \tilde{\mu}_o/\sqrt{\rho\sigma R}$, is the Ohnesorge number which characterizes the relative importance of viscous force to surface tension force, and $G \equiv g\rho R^2/\sigma$ is the gravitational Bond number which characterizes the relative importance of gravitational force to surface tension force. The stress tensor $\mathbf{T}$ in a generalized Newtonian fluid is given by $\mathbf{T} = -p\mathbf{I} + \mu(\dot{\gamma})[\nabla\mathbf{v} + (\nabla\mathbf{v})^T]$, where p is the pressure and the viscosity function $\mu(\dot{\gamma})$ is discussed below. At the free surface the traction boundary condition

$$\mathbf{n} \cdot \mathbf{T} = \frac{1}{Oh} 2H\mathbf{n} \tag{4}$$

and the kinematic boundary condition

$$\mathbf{n} \cdot \mathbf{v} = \mathbf{n} \cdot \mathbf{v_s} \tag{5}$$

apply. Here $\mathbf{n}$ is an outward unit normal to and $2H$ is the twice the local mean curvature of and $\mathbf{v_s}$ is the velocity of points on the interface. In cylindrical coordinates (r, z) with the origin placed along the axis of symmetry and where z is the axial coordinate measured along the axis of symmetry and r is the radial coordinate, $2H$ is given by

$$2H = \frac{1}{h(1+h_z^2)^{1/2}} - \frac{h_{zz}}{(1+h_z^2)^{3/2}} \tag{6}$$

where $r = h(z,t)$ is the interface shape function and subscript z denotes differentiation with respect to z.

In this paper, the shear-thinning behavior is described by a three-parameter Carreau model (see [24]) similar to the one previously used by YB :

$$\mu = (1-\beta)[1+(\alpha\dot{\gamma})^2]^{((n-1)/2)} + \beta \tag{7a}$$

Two different limiting forms of the Carreau model are of interest here. In the so-called power law limit where $\beta \to 0$ and $(\alpha\dot{\gamma})^2 \gg 1$,

$$\mu = |\alpha\dot{\gamma}|^{(n-1)} \tag{7b}$$

When the deformation rate is either vanishingly small or indefinitely large, the Carreau model approaches the following two Newtonian limits

$$\lim_{\dot{\gamma}\to 0} \quad \mu = 1 \tag{7c}$$

$$\lim_{\dot{\gamma}\to \infty} \quad \mu = \beta \tag{7d}$$

In cylindrical coordinates, the magnitude of the deformation rate is given by

$$\dot{\gamma} = \sqrt{2\left(\frac{\partial v_r}{\partial r}\right)^2 + 2\left(\frac{v_r}{r}\right)^2 + \left(\frac{\partial v_r}{\partial z} + \frac{\partial v_z}{\partial r}\right)^2 + 2\left(\frac{\partial v_z}{\partial z}\right)^2} \tag{8}$$

In eq. (8), v_r and v_z denote radial and axial components of the velocity.

Equations (2) - (7a) can be simplified by substituting the following expansions of the unknown axial velocity and pressure in power series in the radial coordinate r, viz.

$$v_z(r,z,t) = v_0(z,t) + v_2(z,t)r^2 + \ldots, \tag{9}$$

$$p(r,z,t) = p_0(z,t) + p_2(z,t)r^2 + \ldots \tag{10}$$

and retaining only the leading order terms in the resulting expressions, as described by Eggers and Dupont [27] for Newtonian fluids. As shown by YB, the following set of 1-D nonlinear evolution equations for $h(z,t)$ and $v \equiv v_0(z,t)$ then results:

$$\frac{\partial v}{\partial t} + v\frac{\partial v}{\partial z} = -\frac{\partial\,(2H)}{\partial z} + \frac{3Oh}{h^2}\left[\frac{\partial}{\partial z}\left(\mu^{(0)}h^2\frac{\partial v}{\partial z}\right)\right] - G \tag{11}$$

$$\frac{\partial h}{\partial t} + v\frac{\partial h}{\partial z} = -\frac{h}{2}\frac{\partial v}{\partial z} \tag{12}$$

$$\mu = \left[(1-\beta)\left(\sqrt{1+3\alpha^2\left(\frac{\partial v}{\partial z}\right)^2}\right)^{(n-1)} + \beta\right] + \mathcal{O}(r^2) = \mu^{(0)} + \ldots, \tag{13}$$

where $\mu^{(0)}$ is the leading-order term in the Taylor series expansion of the viscosity. In the power law limit, it follows from eqs. (7b) and (13) that

$$\mu^{(0)} = \left| \sqrt{3}\alpha \frac{\partial v}{\partial z} \right|^{(n-1)} \tag{14}$$

The heretofore used nondimensionalization is inappropriate in the creeping flow limit as the density does not enter the problem. In this situation, while it is still appropriate to use R as characteristic length, one must instead employ $\sigma/\tilde{\mu}_o$ as characteristic velocity or $R\tilde{\mu}_o/\sigma$ as characteristic time. The resulting set of 1-D evolution equations are identical to (11) and (12) with the following exceptions. First, the two terms corresponding to the local and convective accelerations on the left side of equation (11) do not arise because they are premultiplied by Oh^{-2} and in the creeping flow limit $Oh^{-1} \to 0$. Second, the viscous term on the right side of (11) gets premultiplied by unity rather than Oh in this limit. Therefore, the properly nondimensionalized 1-D momentum equation in the creeping flow limit becomes:

$$0 = -\frac{\partial(2H)}{\partial z} + \frac{3}{h^2}\left[\frac{\partial}{\partial z}\left(\mu^{(0)} h^2 \frac{\partial v}{\partial z}\right)\right] - G \tag{15}$$

In the computational results to be presented in section 5, the bridge length L is held fixed and the deformation and breakup of the bridge are driven by subjecting the bridge to an initial deformation having finite amplitude. In this situation, it is convenient to place the origin of the cylindrical coordinate system at the center of the bridge. The 1-D evolution

equations are then solved subject to the following boundary conditions imposed at the two rods holding the bridge captive:

$$\begin{aligned} h(L/2,t) &= 1\,, \quad v(L/2,t) = 0 \\ h(-L/2,t) &= 1\,, \quad v(-L/2,t) = 0 \end{aligned} \tag{16}$$

3 Numerical Analysis

The governing set of 1-D eqs. (11) and (12) or (15) and (12) is solved numerically by a method of lines using the Galerkin/finite element method (G/FEM) for spatial discretization and an adaptive finite difference method for temporal discretization [28]. The algorithm used here is almost identical to that used by YB but with the following difference. In the present work, all unknowns are represented in terms of quadratic basis functions rather than the linear ones used in YB. Further details on the numerical method can be found in YB.

As will be shown in section 5, there are several points in the pinch region where $\partial v/\partial z = 0$. Therefore, the viscosity in the power law model (cf. eq. (14)) is non-differentiable at these points but the derivative of the viscosity appears in the slender-jet equations (cf. eq. (11) or (15)). Fortunately, the use of the G/FEM overcomes this difficulty. The Galerkin weighted residuals of eq. (11) or (15) are constructed by multiplying eq. (11) or (15) by the basis functions and integrating the resulting expressions over the computational domain. The

term involving the viscosity is then integrated by parts, thereby obviating the need for differentiating the viscosity. By contrast, a finite difference algorithm would have considerable difficulty in dealing with this situation.

4 Self-similar solution for power law fluid

4.1 Viscous power law regime

The 1-D momentum equation governing the pinch-off of a thread of a power law fluid undergoing creeping flow can be obtained by substituting eq. (14) for the viscosity $\mu^{(0)}$ in eq. (15). Following the analysis of Papageorgiou [11] for pinching of viscous Newtonian threads, $h(z,t)$ and $v(z,t)$ are expected to have the following self-similar forms as $\tau \to 0$, where τ is the time remaining to breakup:

$$h(z',\tau) = \tau^{\alpha_1}\phi(\xi) \tag{17}$$

$$v(z',\tau) = \tau^{\alpha_2}\psi(\xi) \tag{18}$$

where

$$z' = z - z_o \tag{19}$$

$$\tau = t_o - t \tag{20}$$

$$\xi = z'/\tau^{\delta} \tag{21}$$

Here z_o is the axial location of the pinch-off singularity, t_o is the breakup time, and z' is the axial coordinate measured from z_o. The exponent δ controls the extent of the similarity region and ξ is the similarity variable. In addition to δ, the exponents α_1 and α_2 and the scaling functions $\phi(\xi)$ and $\psi(\xi)$ are to be determined as part of the analysis.

Inserting eqs. (17) and (18) in eqs. (15) and (12) and enforcing the time invariance of these equations results in a coupled set of ordinary differential equations for the scaling functions $\phi(\xi)$ and $\psi(\xi)$

$$\left(3\left|\sqrt{3}\alpha\psi'\right|^{(n-1)}\psi'\phi^2 + \phi\right)' = 0, \tag{22}$$

$$\phi' = \phi\frac{n - \psi'/2}{\psi + \delta\xi} \tag{23}$$

where primes denote differentiation with respect to ξ and the scaling exponents $\alpha_1 = n$ and $\alpha_2 = \delta - 1$. When $n = 1$, eqs. (22) and (23) reduce to the equations governing the self-similar pinch-off of a thread of a viscous Newtonian fluid [11]. The scaling functions ϕ and ψ, and the axial scaling exponent δ, are determined below. It has been shown by Renardy [21] that the pinch-off dynamics of a power law fluid are qualitatively similar to those of a Newtonian fluid under conditions of creeping flow. Moreover, Renardy has also noted that in contrast

to the Newtonian case, a closed form solution for δ does not exist and has to be determined numerically in the non-Newtonian case.

The denominator of the kinematic boundary condition, eq. (23), vanishes when $\psi(\xi) = -\delta\xi$ at a value of the similarity variable $\xi = \xi_0$. Therefore, as in the Newtonian case, smooth solutions only exist if at $\xi = \xi_0$

$$\psi(\xi_o) = -\delta\xi_o \tag{24}$$

$$\psi'(\xi_o) = 2n \tag{25}$$

The numerical evaluation of δ is facilitated by expanding ϕ and ψ in a Taylor series in ξ about $\xi = \xi_o$, which turns out to be the pinch-off stagnation point (see below). The local expansions can be written as

$$\phi(\xi - \xi_o) = \phi_0 + \phi_2(\xi - \xi_o)^2 + \phi_4(\xi - \xi_o)^4 + \dots \tag{26}$$

$$\psi(\xi - \xi_o) = -\delta\xi_o + 2n(\xi - \xi_o) + \psi_3(\xi - \xi_o)^3 + \dots \tag{27}$$

where $\phi_0, \phi_2, \dots$ and $\psi_3, \dots$ are coefficients to be determined. For the case of a Newtonian fluid ($n = 1$) it has been shown that the scaling function ϕ is even and the scaling function ψ is odd [11] and also that $\xi_o = 0$ [29]. Similar results also hold for a power law fluid. It follows from eqs. (22) and (23) and eqs. (26) and (27) that

$$\phi_0 = \frac{1}{6}\frac{1}{3^{(n-1)/2}\alpha^{n-1}(2n)^n(2n + \delta - 1)} \tag{28}$$

Therefore, using eqs. (17) and (26) the minimum thread radius can be shown to vary with time to breakup as

$$h_{min}(t) = \phi_0 \tau^n \tag{29}$$

Equations (28) and (29) along with the value of ϕ_0 obtained from numerical solution of the complete slender-jet equations will provide one of several ways to calculate the value of δ in section 5.1.

Eq. (22) represents the balance between capillary and viscous forces, assuming that inertial force is small. This regime is henceforward referred to as the viscous power law or the VP regime. The validity of the assumption that inertia is negligible can be checked only if the value of δ is known. However, it is well-known from the pinch-off of Newtonian jets that neglecting inertia is asymptotically inconsistent as breakup is approached, and the V regime gives way to the IV regime. The analogous transition will be more pronounced for a power law fluid. Hence, inertial effects must be included in the analysis of pinch-off of non-Newtonian fluids.

4.2 Inertial-viscous power law regime

When inertial, viscous, and capillary forces are all of the same order, Eggers[7] has shown that the appropriate characteristic length and time units close to breakup are the viscous length scale and the viscous time scale. In the present case, these scales are given by $l_\nu = \tilde{\mu}_o^2/\rho\sigma$ and

$t_\nu = \tilde{\mu}_o^3/\rho\sigma^2$, respectively. Therefore, the appropriately scaled equations governing the axial velocity and the shape function are virtually identical to eqs. (11) and (12) except Oh in eq. (11) is replaced by unity. Following the analysis of Eggers [7] for pinching of Newtonian threads when inertia cannot be neglected, the shape function $h(z,t)$ and the axial velocity $v(z,t)$ are expected to have the self-similar forms given once again by eqs. (17) and (18) as $\tau \to 0$. Inserting eqs. (17) and (18) in eq. (11) and eq. (12) and enforcing the time invariance of these equations results in a coupled set of ordinary differential equations for the scaling functions $\phi(\xi)$ and $\psi(\xi)$

$$n\psi/2+(1-n/2)\xi\psi'+\psi\psi' = \phi'/\phi^2+\sqrt{3}^{(n+1)}(|\alpha\psi'|^{(n-1)}\,\psi')'+2\sqrt{3}^{(n+1)}\,|\alpha\psi'|^{(n-1)}\,\psi'\phi'/\phi \quad (30)$$

$$\phi' = \phi\frac{n-\psi'/2}{\psi+(1-n/2)\xi} \quad (31)$$

with unique scaling exponents

$$\alpha_1 = n, \quad \alpha_2 = -n/2, \quad \delta = 1-n/2 \quad (32)$$

When $n = 1$, eqs. (30) and (31) reduce to the equations governing the self-similar pinch-off of a thread of a Newtonian fluid in the IV regime [7]. Equation (30) represents the balance between inertial, viscous, and capillary forces, with all three terms diverging as $\tau^{(-n/2-1)}$ as

$\tau \to 0$. Since $h \sim \tau^n$ and $z' \sim \tau^{1-n/2}$ (cf. eqs. (17), (21), and (32)), both radial and axial length scales vary as $\tau^{2/3}$ when $n = 2/3$. Therefore, the 1-D theory will fail for values of n below 2/3, as close to breakup the axial length scale will become smaller than the radial length scale and the thread will no longer be slender. For such cases, a full 2-D theory is needed for studying the pinch-off dynamics. Discussion of such a theory is outside of the scope of this paper.

4.3 Determination of similarity solutions

Scaling functions ϕ and ψ can be determined in one of two ways. The first approach is to determine similarity solutions directly by solving eqs. (22) and (23) or eqs. (30) and (31) by a shooting method, as done by Eggers [8], Brenner et al. [29], and Papageorgiou [11] for Newtonian fluids. The second approach, which is adopted in section 5, entails collapsing profiles of both the bridge shape and the axial velocity in the vicinity of the axial location where the bridge radius is minimum by rescaling of the transient profiles obtained from numerical solution of the slender-jet equations, viz. eqs. (15) and (12) or eqs. (11) and (12), with the radial and axial scalings deduced in this section.

5 Results

All the numerical results to be reported in this section have been obtained using the 1-D code described in section 3 with 25000 non-uniformly spaced quadratic elements. The following initial condition has been used in all the simulations:

$$h(z,0) = 1 - a\cos\left(\frac{\pi z}{L}\right), -L/2 \leq z \leq L/2 \tag{33}$$

$$v(z,0) = 0, \quad -L/2 \leq z \leq L/2 \tag{34}$$

where $0.2 \leq a \leq 0.8$ is the amplitude of the initial shape perturbation. Moreover, in all of the results to be reported, the bridge length $L = 5$. Simulations have also been carried out for $2 \leq L \leq 9$ and it has been shown that the value of L, as expected, has no effect on the local pinch-off dynamics. The value of the Bond number G equals zero in all the simulations. Values of all the other dimensionless groups are given in the captions to the figures that follow.

5.1 Viscous power law (VP) regime

Figure 3 shows the variation of the computed minimum bridge radius h_{min} with time to breakup τ for a power law fluid under creeping flow conditions. This figure depicts the radial scaling behavior for four different values of the power law exponent ranging between $0.7 \leq n \leq 1$. It is expected from eq. (29) that a pinching bridge of a power law fluid

undergoing creeping flow will exhibit VP scaling where $h_{min} \sim \tau^n$. Figure 3 shows that this is indeed the case when $1 \times 10^{-4} < h_{min} < 1 \times 10^{-2}$. For each n, the computed results lie along a straight line with slope n as predicted by the VP scaling theory. For $n = 1$, h_{min} decreases linearly with τ in accord with the V scaling theory for breakup of a Newtonian thread [11]. The insets to fig. 3 show bridge shapes close to pinch-off in two situations. As expected for $n = 1$ [11], the bridge profile in the vicinity of its center $z = 0$ is quite slender and has the shape of a thin thread. However, fig. 3 also shows that both the length of the thread and the slenderness are lower for $n = 0.7$ compared to those for $n = 1$. These effects can be attributed to shear-thinning of a power law fluid, a point that will be discussed in detail at the end of this section.

According to the discussion in section 4.1, the value of the axial scaling exponent δ, which sets the scaling behavior of both the axial velocity, $v \sim \tau^{\delta-1}$, and the axial length, $z \sim \tau^{\delta}$, has to be determined using numerical solution of the full slender-jet equations. To demonstrate the calculation of δ, fig. 4 shows the variation with τ of the axial velocity and axial distance from the pinch-off singularity at an axial location where $h = 2h_{min}$, viz. $v_{2h_{min}}$ and $(z_{2h_{min}} - z_o)$, for $n = 0.8$. Figure 4 makes plain that $(z_{2h_{min}} - z_o) \sim \tau^{0.293}$ and $v_{2h_{min}} \sim \tau^{-0.707}$, so that both relations predict a value of δ of 0.293. It has been confirmed by direct calculation that the same scalings and the same value of δ result if the axial velocity and the axial length scalings are evaluated at an axial location where $h = 3h_{min}$ and $5h_{min}$.

Moreover, substituting the value of the vertical intercept of h_{min} obtained from fig. 4 in eq. (28) (cf. eq. (29)) also gives a value of δ of 0.293, in accord with VP scaling theory. Figure 4 also shows the variation with τ of the minimum radius h_{min} and the local viscosity $\mu_{h_{min}}$ at the axial location where $h = h_{min}$. The value of $\mu_{h_{min}}$ decreases with τ with a slope of 0.2, in accord with VP scaling theory which predicts that $\mu \sim \tau^{1-n}$.

The radial and axial scalings obtained in the manner described above can then be used to compute the scaling functions ϕ and ψ from numerically calculated local shapes and axial velocity profiles, respectively. Figures 5 and 6 show the results of numerical calculations that give the variation of $\phi \equiv h/\tau^n$ and $\psi \equiv v/\tau^{\delta-1}$ with the similarity variable $\xi \equiv (z - z_o)/\tau^\delta$ in the vicinity of the pinch point where the minimum radius varies as $5.99 \times 10^{-3} > h_{min} > 1.83 \times 10^{-4}$. These figures show that, there is a very good collapse of profiles for $\phi(\xi)$, fig. 5, and $\psi(\xi)$, fig. 6, onto a single curve, which indicates the convergence of numerical solutions to the similarity solutions and occurrence of self-similarity. The two insets to fig. 5 show the global and the local bridge shapes in the vicinity of the pinch point. Similarly, the two insets to fig. 6 show the divergence with time of the axial velocity fields within bridges both from a global and a local perspective. The scaling functions ϕ and ψ are even and odd functions, respectively, about the pinch point, and are qualitatively similar to the scaling functions computed by Papageorgiou [11] for a viscous Newtonian thread.

Figure 7 shows the variation of the axial scaling exponent δ, calculated by three different methods, with the power law exponent n. In fig. 7, δ calculated from the slope of $(z_{2h_{min}} - z_o)$ versus τ is denoted by δ_z. The value of δ calculated from the slope of $v_{2h_{min}}$ versus τ is denoted by δ_v. Finally, values of δ calculated by substituting values of ϕ_0, which are determined from numerical solution of the full slender-jet equations and tabulated in table 1, into the analytical expression given in eq. (28) are denoted by δ_c. Figure 7 makes plain that values of δ_z, δ_v, and δ_c for different n are in excellent agreement when $0.675 \leq n \leq 1$. Moreover, fig. 7 shows that as the value of n falls from 1 to 0.675, the value of δ rises from 0.175 to 0.405. Similarly, table 1 shows that as n falls, ϕ_0 rises. This effect can be attributed to the shear-thinning nature of a power law fluid because the lower the value of n is, the faster are (i) the rate at which the local viscosity μ decreases and consequently (ii) the rate at which the pinch-region thins.

Equation (28) can be rearranged as

$$\delta = \frac{1}{6} \frac{1}{(\sqrt{3}\alpha)^{n-1}(2n)^n \phi_0} + (1 - 2n) \tag{35}$$

A deeper understanding of the effects of shear-thinning on the axial scaling exponent δ can be gained by treating n and ϕ_0 in eq. (35) temporarily as independent variables.

(1) The effect of the power law exponent n on δ can be seen by partial differentiating eq. (35) w.r.t. n:

$$\frac{\partial \delta}{\partial n} = \frac{-1}{6\phi_0}\left\{12\phi_0 + (2n)^{-n}(\sqrt{3}\alpha)^{1-n}\left[1 + \log\left(2\sqrt{3}\alpha n\right)\right]\right\} \tag{36}$$

Since $\phi_0 > 0$, the sign of $\frac{\partial \delta}{\partial n}$ in eq. (36) depends on the ranges of values of n and α. If the power law exponent is restricted as $0.15 < n < 1$, the power law time constant has to be $\alpha \geq 1$ so that $\frac{\partial \delta}{\partial n} < 0$. If the lowest value of n is decreased below 0.15, the lowest allowable value of α has to be increased above unity to ensure that $\frac{\partial \delta}{\partial n} < 0$.

(2) The effect of variations in the prefactor ϕ_0 on δ can be seen by partial differentiating eq. (35) w.r.t. ϕ_0:

$$\frac{\partial \delta}{\partial \phi_0} = \frac{-1}{6{\phi_0}^2}(2n)^{-n}(\sqrt{3}\alpha)^{n-1} \tag{37}$$

Since $\phi_0 > 0$, eq. (37) shows that $\frac{\partial \delta}{\partial \phi_0} < 0$ for $n > 0$ and $\alpha > 0$.

Further insights into the dependence of the axial scaling exponent δ on the power law exponent n can be gained by carrying out a Taylor series expansion of δ about its Newtonian limit, $n = 1$. Letting, $\epsilon \equiv 1 - n \ll 1$, it can be shown from eq. (35) that

$$\delta(1-\epsilon) = 0.175 + \left[4.634 + 16.554\left(\frac{\mathrm{d}\phi_0}{\mathrm{d}n}\right)_{n=1}\right]\epsilon + O(\epsilon^2) \tag{38}$$

The higher-order terms in the above expansion involve higher-order derivatives of ϕ_0 w.r.t. n. Evaluation of eq. (38) requires the calculation of $\left(\frac{\mathrm{d}\phi_0}{\mathrm{d}n}\right)_{n=1}$ and higher-order derivatives of ϕ_0 w.r.t. n evaluated at $n = 1$. In order to do so, the data of table 1 are least-square fitted by a third-order polynomial :

$$\phi_{03} = -0.2848n^3 + 1.4023n^2 - 2.189n + 1.1425 \tag{39}$$

Values of δ calculated in this manner by a third-order expansion in ϵ are denoted by δ_e and tabulated in table 2. Table 2 shows that values of δ calculated by perturbation expansion, δ_e, and those obtained from computation agree well. The agreement between them can of course be improved by including higher-order terms in the expansion of eq. (38) but is not pursued here as the principal goal behind carrying out the Taylor series expansion is to expose the competing effects of shear-thinning behavior on δ rather than providing a fourth method of quantitatively determining δ.

Figure 7 shows that the agreement between values of the axial scaling exponent δ obtained by the three methods deteriorates for values of $n < 0.675$. This effect may be attributable to two causes: loss of local slenderness, as discussed in the next paragraph, and neglect of inertial terms in the axial momentum balance, as discussed in the paragraph after the next one.

The local slenderness of a thinning thread at a given time τ is given by the ratio of the axial to the radial length scale, viz. $h/z' \sim \tau^{n-\delta}$. Since δ increases as n decreases, thinning threads become less slender as n decreases from the Newtonian limit of $n = 1$. Therefore, when the value of n falls below a critical value, the slender-jet approximation will fail and a full 2-D theory will be required. Figure 8 shows the scaling function $\phi(\xi)$ that has been

calculated numerically for $n = 0.7, 0.8, 0.9$ and 1. Figure 8 makes clear that $\phi(\xi)$ is an even function for all values of n. Moreover, as n decreases, the shapes become less slender in the vicinity of $\xi = 0$, in accord with the results of the VP scaling theory.

After calculating δ for different values of n, the magnitude of the neglected inertial terms in the momentum balance can be estimated to test the consistency of the creeping flow assumption as pinch-off is approached. The ratio of inertial and viscous stresses can be characterized by a local Reynolds number $Re \equiv \rho\tilde{v}\tilde{z}/\tilde{\mu}$. According to the results of section 4.1, the local Reynolds number can be expressed as

$$Re = \frac{\rho(v_i\tau^{\delta-1})(z_i\tau^{\delta})}{(\mu_i\tau^{1-n})} = \frac{\rho v_i z_i}{\mu_i}\tau^{2\delta+n-2} = Re_o\tau^{2\delta+n-2}$$

where the quantities with the subscripts "i" denote the initial values of the axial velocity, axial length, and viscosity, and Re_o is the initial value of the Reynolds number. Choosing the values of v_i and z_i as those appropriate for creeping flow (cf. section 2), viz. $v_i = \sigma/\tilde{\mu}_o$ and $z_i = R$, and setting the value of the initial viscosity equal to the zero-shear-rate viscosity, viz. $\mu_i = \tilde{\mu}_o$, it follows that $Re_o = Oh^{-2}$. For $0.67 < n < 1$, it can be seen from fig. 7 that $0.4 > \delta > 0.175$ and therefore $-0.57 > 2\delta + n - 2 > -0.65$. Hence, neglect of inertia is invalid as $\tau \to 0$. Therefore any balance close to pinch-off must include inertial terms, a fact which has already been shown to be true during Newtonian jet breakup [30].

5.2 Inertial-viscous power law (IVP) regime

Figure 9 shows the variation of the computed minimum bridge radius h_{min} with time to breakup τ for a power law bridge when $Oh = 0.1$. This figure depicts the radial scaling behavior for four different values of n ranging between 0.7 to 1. The dynamical response of the bridge close to pinch-off is expected to follow IVP scaling where $h_{min} \sim \tau^n$ (cf. section 4.2). Figure 9 shows that this is indeed the case when $1 \times 10^{-4} < h_{min} < 1 \times 10^{-2}$. For each n, the computed results lie along a straight line with slope n as predicted by IVP scaling theory. The insets to fig. 9 show shapes of two bridges, one with $n = 1$ and the other with $n = 0.7$, at two different stages of their evolution. The profiles of both bridges are symmetric about $z_{h_{min}}$ initially but become asymmetric as pinch-off nears. Figure 10 shows the corresponding variation with τ of minimum bridge radius h_{min}, axial distance from the breakup singularity $(z_{2h_{min}} - z_o)$, axial velocity $v_{2h_{min}}$, and local viscosity $\mu_{h_{min}}$ for a liquid bridge with $n = 0.7$ and $Oh = 0.1$. This figure makes plain that $h_{min} \sim \tau^{0.7}$, $(z_{2h_{min}} - z_o) \sim \tau^{0.65}$, $v_{2h_{min}} \sim \tau^{-0.35}$ and $\mu_{h_{min}} \sim \tau^{0.3}$, which are all in accord with predictions of IVP scaling theory (cf. section 4.2).

The radial and axial scalings obtained in section 4.2 can be used to compute the scaling functions $\phi(\xi)$ and $\psi(\xi)$ from numerically calculated local shapes and axial velocity profiles, respectively. Figure 11 shows the results of numerical computations that give the variation of the shape function $\phi \equiv Oh^{3n-2}h/\tau^n$ with the similarity variable $\xi \equiv Oh^{1-3n/2}(z - z_o)/\tau^{1-n/2}$

in the vicinity of the pinch point when $2.3 \times 10^{-2} > h_{min} > 7.03 \times 10^{-4}$. Here the prefactors of Oh^{3n-2} and $Oh^{1-3n/2}$ arise because of the difference in the nondimensionalization of the equations governing the global dynamics presented in section 2, which uses the rod radius and the capillary time as characteristic length and time, and that of the equations governing the local dynamics presented in section 4.2, which uses the viscous length and time scales as the corresponding characteristic scales (see, for example, the work of Chen *et al.* [14]). Similarly, fig. 12 shows the variation of the velocity function $\psi(\xi) \equiv Oh^{3n/2-2} v/\tau^{-n/2}$ with ξ in the vicinity of the pinch point when $1.41 \times 10^{-3} > h_{min} > 1.68 \times 10^{-4}$. Figures 11 and 12 show that there is a very good collapse of profiles for $\phi(\xi)$, fig. 11, and $\psi(\xi)$, fig. 12, which supports that the dynamics close to pinch-off is indeed self-similar. Figure 11 also shows that $\phi(\xi)$ is asymmetric about the pinch point which is qualitatively similar to the scaling function computed by Eggers for a Newtonian thread [8].

Figure 13 shows the scaling function $\phi(\xi)$ that has been computed numerically for $n = 0.7, 0.8, 0.9$ and 1. The profile for $n = 1$ is in excellent agreement with the so called Eggers's universal solution for a Newtonian fluid [8]. As discussed in section 4.2 and shown by fig. 13, the local slenderness decreases as n decreases. According to IVP scaling theory, the ratio of radial to axial scaling varies as $\tau^{3n/2-1}$ (cf. eq. (32)). Therefore, when $n = 2/3$, close to pinch-off the local filament shape becomes conical and results in the failure of the 1-D theory.

5.3 Change in scaling from VP to IVP

It has been shown at the end of section 5.1 that even in the case of a thinning thread of a high viscosity fluid initially exhibiting VP scaling, the local Reynolds number does not remain small for all time and therefore inertia becomes important as pinch-off is approached. It has subsequently been demonstrated in section 5.2 that the final scaling regime before pinch-off involves a balance between viscous, inertial, and capillary forces. The value of the minimum bridge radius h_{min} at which the transition from the initial VP scaling regime to the final IVP scaling regime occurs can be determined as follows. As shown in section 5.1, the local Reynolds number in a thinning thread of a high viscosity fluid initially undergoing creeping flow is given by $Re = Re_o \tau^{2\delta+n-2} = Oh^{-2}\tau^{2\delta+n-2}$. Transition from VP scaling to IVP scaling should occur when $Re = \mathcal{O}(1)$. In terms of time remaining to breakup, the transition should therefore occur when $\tau = Re_o^{1/(2-2\delta-n)}$. Since $h \sim \tau^n$, the value of the minimum thread radius at the transition is given by

$$h_{min} \sim Re_o^{n/(2-2\delta-n)} = Oh^{2n/(2\delta+n-2)}. \tag{40}$$

Figure 14 shows the variation with τ of the computed minimum bridge radius h_{min}, $(z_{2h_{min}} - z_o)$, $v_{2h_{min}}$, and $\mu_{h_{min}}$ for a power law bridge with $n = 0.7$ and $Oh = Re_o^{-1/2} = 5$. Figure 14 shows that the calculations initially follow dynamics dictated by VP scaling. It follows from eq. (40), however, that the inertial terms should become important when the minimum

radius decreases to order $Oh^{-1.4/0.54} = Re_o^{0.7/0.54} = 1.5 \times 10^{-2}$. Figure 14 shows that the transition begins when $h_{min} \sim 2 \times 10^{-3}$ and the dynamics thereafter crosses over to IVP scaling. First, a similar change in scaling has been shown albeit experimentally for a viscous Newtonian fluid undergoing pinch-off by Rothert et al. [12]. Second, the value of the minimum thread radius at which the dynamics transitions from VP scaling to IVP scaling predicted from the computations (cf. fig. 14)) is almost an order of magnitude smaller than the corresponding value predicted from eq. (40). Chen et al. [14] have shown both experimentally and computationally that the measured and computed values of h_{min} for transition from PF scaling to IV scaling for Newtonian fluids also exhibits the same behavior.

5.4 Scaling for a Carreau fluid

Having demonstrated the self-similar behavior of a bridge of a power law fluid during pinch-off, attention is now turned to the pinch-off dynamics of a liquid bridge of a Carreau fluid. Figure 15 shows the variation of the computed minimum bridge radius h_{min} with time τ to breakup for a bridge of a Carreau fluid with $n = 0.2, 0.4$, and 0.6. All the other relevant dimensionless groups are given in the caption to the figure. Figure 15 shows that in each case, $h_{min} \sim \tau^n$ initially, in agreement with results expected of a power law fluid as described in the previous section. As pinch-off continues, fig. 15 shows that the dynamics undergoes a transition and the power law scaling regime gives way to a Newtonian scaling regime. In

the power law regime, the Carreau model is well approximated by eq. (7b) appropriate for a power law fluid. Similarly, in the final Newtonian regime, the viscosity predicted by the Carreau model is well approximated by the infinite-shear-rate viscosity β given by eq. (7d). The transition from the power law regime to the Newtonian regime occurs when the magnitude of the viscosity μ predicted by both limiting forms of the Carreau model are of the same order. Therefore, the rate of deformation at the transition is given by

$$\dot{\gamma}_{transition} = \frac{\beta^{1/(n-1)}}{\alpha} \tag{41}$$

It is noteworthy that for a power law fluid, the maximum velocity gradient in the bridge diverges as $\dot{\gamma} \sim \partial v/\partial z' \sim \tau^{-1}$ for any value of n (cf. section 4). Substituting this result into eq. (41) yields the following expression for the time τ before breakup for transition from the power law regime to the Newtonian regime

$$\tau_{transition} = \dot{\gamma}^{-1}_{transition} = \frac{\alpha}{\beta^{1/(n-1)}} \tag{42}$$

Figure 15 also shows that the transition occurs first when $n = 0.2$ followed by $n = 0.4$ and $n = 0.6$, respectively. This trend can be appreciated by noting that eq. (41) or eq. (42) can be differentiated w.r.t. n to give

$$\frac{\partial}{\partial n}\left(\dot{\gamma}_{transition}\right) = -\dot{\gamma}^2_{transition}\frac{\partial}{\partial n}(\tau_{transition}) = -\frac{\beta^{\frac{1}{n-1}}}{(n-1)^2}\frac{\log\beta}{\alpha} \tag{43}$$

For all $0 < \beta < 1$, $\alpha > 0$, and $0 < n < 1$, eq. (43) predicts that $\frac{\partial \dot{\gamma}_{transition}}{\partial n} > 0$ and $\frac{\partial \tau_{transition}}{\partial n} < 0$. Therefore, the smaller the value of n is, the smaller is the value of $\dot{\gamma}_{transition}$

and the larger is the value of $\tau_{transition}$ at which the transition will occur, in accord with the results depicted by the three profiles in fig. 15.

As remarked previously, smaller values of n result in higher rates of shear-thinning. Therefore, it accords with intuition that, for a fixed value of β, the fluid with the smallest value of n shear-thins the fastest and approaches the Newtonian regime the earliest. This expectation is of course confirmed by fig. 16 which shows the computed variation of the local viscosity μ with the local deformation rate $\dot{\gamma}$ at the axial location where the thread radius is smallest for the same three Carreau fluids depicted in fig. 15. All three profiles in fig. 16 show that the viscosity μ exhibits a power law behavior at small values of $\dot{\gamma}$ and finally approaches the inifinite-shear-rate viscosity $\beta = 0.01$ at large values of $\dot{\gamma}$. Table 3 shows the values of $\dot{\gamma}_{transition}$ and $\tau_{transition}$ predicted by eqs. (41) and (42), respectively, and order of magnitude estimates for the same quantities obtained from the computed profiles of μ versus $\dot{\gamma}$ in fig. 16 and those of h_{min} versus τ in fig. 15. Table 3 makes plain that the predicted values are in good agreement with the computed values. Hence, eqs. (41) and (42) provide good *a priori* estimates of the values of $\dot{\gamma}_{transition}$ and $\tau_{transition}$ for transition from power law scaling to Newtonian scaling behavior for a Carreau fluid. Examination of the profiles of bridges near breakup under the conditions of figs. 15 and 16 reveals yet another interesting consequence of the effect of n on the bridge dynamics. The insets to fig. 15 show bridge shapes at the incipience of pinch-off when $h_{min} = 1 \times 10^{-5}$. Since the fluid with the

smallest value of n approaches the Newtonian regime the earliest, it accords with intuition that the bridge with $n = 0.2$ forms a slender thread in its middle as pinch-off nears.

Figure 17 shows the variation of the computed minimum bridge radius h_{min} with time to breakup τ for a bridge of a Carreau fluid with $\beta = 0.1, 0.01$, and 0.001. All the other relevant dimensionless groups are given in the caption to the figure. Figure 17 makes plain that the larger the value of β is, the sooner the transition occurs from power law scaling to Newtonian scaling. This trend also can be appreciated by differentiating eq. (41) or eq. (42) w.r.t. β to give

$$\frac{\partial}{\partial\beta}\left(\dot{\gamma}_{transition}\right) = -\dot{\gamma}^2_{transition}\frac{\partial}{\partial\beta}(\tau_{transition}) = -\frac{1}{(1-n)}\frac{\beta^{\frac{2-n}{n-1}}}{\alpha} \tag{44}$$

For all $0 < \beta < 1$, $\alpha > 0$ and $0 < n < 1$, eq. (44) predicts that $\frac{\partial\dot{\gamma}_{transition}}{\partial\beta} < 0$ and $\frac{\partial\tau_{transition}}{\partial\beta} > 0$. Therefore, the smaller the value of β is, the larger is the value of $\dot{\gamma}_{transition}$ and the smaller is the value of $\tau_{transition}$ at which the transition will occur.

At a fixed value of n, a Carreau fluid can shear-thin most for the smallest value of β, thereby resulting in a delayed transition in a fluid with small β compared to one with large β. This expectation is of course confirmed by fig. 18 which shows the computed variation of the local viscosity μ with the local deformation rate $\dot{\gamma}$ at the axial location where the thread radius is smallest for the same three Carreau fluids depicted in fig. 17. All three profiles in fig. 18 show that the viscosity μ exhibits a power law behavior at small values of $\dot{\gamma}$ and

finally approaches the infinite-shear-rate viscosity β at large values of $\dot{\gamma}$. Table 4 shows the values of $\dot{\gamma}_{transition}$ and $\tau_{transition}$ predicted by eqs. (41) and (42), respectively, and order of magnitude estimates for the same quantities obtained from the computed profiles of μ versus $\dot{\gamma}$ in fig. 18 and those of h_{min} versus τ in fig. 17. Table 4 makes plain that the predicted values are in good agreement with the computed values. Hence, once again, eqs. (41) and (42) provide good *a priori* estimates of the values of $\dot{\gamma}_{transition}$ and $\tau_{transition}$ for transition from power law scaling to Newtonian scaling behavior for a Carreau fluid.

6 Conclusions

In this paper, a detailed study of capillary thinning of generalized Newtonian fluids has been carried out to improve the understanding of the role of shear-thinning rheology on the local pinch-off dynamics. The study has relied on (a) computing numerical solutions to the full 1-D slender-jet equations for a breaking liquid bridge and (b) asymptotic analysis of the 1-D equations to capture the local pinch-off dynamics for fluids whose rheology are described by power law and Carreau models. The dynamics of a necking bridge of a power law fluid undergoing creeping flow is driven by a balance between viscous and capillary forces alone and exhibits self-similar behavior close to pinch-off. The scaling exponents for the neck radius and the axial velocity are found to be unique for a given value of the power law

exponent n. The value of the axial scaling exponent δ is determined in several ways using a combination of numerical solution of the governing 1-D equations and analytical methods. Values of δ determined by the different methods are shown to be in excellent agreement with one another. The local shapes and axial velocity computed by numerical solution of the full 1-D slender-jet equations without inertia show self-similar behavior. The local shape and axial velocity profiles are found to be qualitatively similar to ones found by Papageorgiou [11] in his study of pinch-off of Newtonian jets undergoing Stokes flow.

Furthermore, it is shown here that close to pinch-off, inertia becomes important and alters the dynamics, just as in the case of Newtonian threads undergoing capillary pinching [8]. The dynamics of a bridge of a power law fluid that is driven by a balance between inertial, viscous, and capillary forces also exhibits self-similar behavior close to pinch-off. The scaling exponents are uniquely determined once a self- similar transformation of the governing 1-D equations is carried out. Once again, the local shape and axial velocity profiles computed by numerical solution of the full 1-D slender-jet equations show self-similar behavior. Inertia results in the local shapes near pinch-off becoming asymmetric about the axial location where the thread radius is a minimum, as in the problem of Newtonian jet breakup [7, 8]. Due to loss of local slenderness, the 1-D slender-jet equations do not remain faithful to the fluid physics for values of the power law exponent $n \leq 2/3$.

For threads of Carreau fluids undergoing capillary pinching, two distinct scaling regimes are observed. These are an initial power law scaling regime which gives way to a final Newtonian scaling regime as pinch-off nears. It is shown that the deformation rate and the time at which the transition from power law to Newtonian scaling occur can be estimated by simple expressions involving the rheological parameters. The predictions of these expressions are demonstrated to agree well with those of numerical simulations of the 1-D equations.

There are several areas of future research that can be carried out to extend the analyses and results presented in this paper. One obvious extension entails computation of similarity solutions directly from the equations governing the scaling functions ϕ and ψ in the self-similar space (cf. eqs. (22) and (23) or eqs. (30) and (31)) in contrast to the approach adopted here. The second involves solving the full set of equations governing the dynamics of capillary thinning of generalized Newtonian fluids, as in YB, albeit using more robust algorithms (see, for example, references [13, 14]) than that used by YB to enable computation of interface shapes that can overturn prior to rupture. Indeed, such analyses are needed to resolve the fate of a breaking fluid thread when the interface profile is not slender, as in the case of a generalized Newtonian fluid with a power law exponent $n \leq 2/3$.

Acknowledgements

The Purdue authors thank the Chemical Sciences Division of the Office of Basic Energy Sciences of the US DOE and the 3M and the Eastman Kodak companies for support of this research. GHM would like to acknowledge the support of the Schlumberger Foundation for studies of capillary breakup of complex fluids.

References

[1] O. A. Basaran, Small-scale free surface flows with breakup: Drop formation and emerging applications, AIChE J. **48**, 1842 (2002).

[2] M. Döring, Ink-jet printing, Philips. Tech. Rev. **40**, 192 (1982).

[3] M. M. Denn, Drawing of liquids to form fibers, Annu. Rev. Fluid Mech. **12**, 365 (1980).

[4] G. McKinley and T. Sridhar, Filament-stretching rheometry of complex fluids, Annu. Rev. Fluid Mech. **34**, 375 (2002).

[5] J. B. Keller and M. J. Miksis, Surface tension driven flows, SIAM J. Appl. Math **43**, 268 (1983).

[6] D. H. Peregrine, G. Shoker, and A. Symon, The bifurcation of liquid bridges, J. Fluid Mech. **212**, 25 (1990).

[7] J. Eggers, Universal pinching of 3d axisymmetric free-surface flow, Phys. Rev. Lett. **71**, 3458 (1993).

[8] J. Eggers, Theory of drop formation, Phys. Fluids **7**, 941 (1995).

[9] R. F. Day, E. J. Hinch, and J. R. Lister, Self-similar capillary pinchoff of an inviscid fluid, Phys. Rev. Lett. **80**, 704 (1998).

[10] D. T. Papageorgiou, Analytical description of the breakup of liquid jets, J. Fluid Mech. **301**, 109 (1995).

[11] D. T. Papageorgiou, On the breakup of viscous liquid threads, Phys. Fluids **7**, 1529 (1995).

[12] A. Rothert, R. Richter, and I. Rehberg, Transition from symmetric to asymmetric scaling function before drop pinch-off, Phys. Rev. Lett. **87**, 4501 (2001).

[13] P. K. Notz, A. U. Chen, and O. A. Basaran, Satellite drops: Unexpected dynamics and change of scaling during pinch-off, Phys. Fluids **13**, 549 (2001).

[14] A. Chen, P. K. Notz, and O. A. Basaran, Computational and experimental analysis of pinch-off and scaling, Phys. Rev. Lett. **13**, 549 (2002).

[15] M. Goldin, P. Yerushalmi, R. Pfeffer, and R. Shinnar, Breakup of a laminar capillary jet of a viscoelastic filaments, J. Fluid Mech. **38**, 689 (1969).

[16] J. M. Y. Amarouchene, D. Bonn and H. Kellay, Inhibition of the finite-time singularity during droplet fission of a polymeric fluid, Phys. Rev. Lett. **86**, 3558 (2001).

[17] O. E. Yildirim and O. A. Basaran, Deformation and breakup of stretching bridges of Newtonian and shear-thinning liquids: comparison of one- and two-dimensional models, Chem. Engng. Sci. **56**, 211 (2001).

[18] J. Cooper-White, J. Fagan, V. Tirtaatmadja, D. Lester, and D. Boger, Drop formation dynamics of constant low-viscosity, elastic fluids, J. Non-Newton. Fluid Mech. **106**, 29 (2002).

[19] M. Renardy, Self-similar breakup of a Giesekus jet, J. Non-Newton. Fluid Mech. **97**, 283 (2001).

[20] M. Renardy, Self-similar jet breakup for a generalized PTT model, J. Non-Newton. Fluid Mech. **103**, 261 (2002).

[21] M. Renardy, Similarity solutions for jet breakup for various models of viscoelastic fluid, J. Non-Newton. Fluid Mech. **104**, 65 (2002).

[22] H.-C. Chang, E. Demekhin, and E. Kalaidin, Iterated stretching of viscoelastic jets, Phys. Fluids **7**, 1717 (1999).

[23] M. Renardy and D. Losh, Similarity solutions for jet breakup in a Giesekus fluid with inertia, J. Non-Newton. Fluid Mech. **106**, 17 (2002).

[24] P. J. Carreau, D. D. Kee, and M. Daroux, An analysis of the viscous behavior of polymeric solutions, Canadian Journal of Chemical Engineering **57**, 135 (1979).

[25] D. Debbaut and M. Crochet, Extensional effects in complex flows, J. Non-Newton. Fluid Mech. **30**, 169 (1988).

[26] S. E. Bechtel, J. Z. Cao, and M. G. Forest, Practical application of a higher-order perturbation-theory for slender viscoelastic jets and fibers, J. Non-Newton. Fluid Mech. **41**, 201 (1989).

[27] J. Eggers and T. F. Dupont, Drop formation in a one–dimensional approximation of the Navier-Stokes equation, J. Fluid Mech. **262**, 205 (1994).

[28] X. Zhang, R. S. Padgett, and O. A. Basaran, Nonlinear deformation and breakup of stretching liquid bridges, J. Fluid Mech. **329**, 207 (1996).

[29] M. P. Brenner, J. R. Lister, and H. A. Stone, Pinching threads, singularities and the number 0.0304, Phys. Fluids **8**, 2827 (1996).

[30] J. R. Lister and H. A. Stone, Capillary breakup of a viscous thread surrounded by another viscous fluid, Phys. Fluids **10**, 2758 (1998).

Correspondence and requests of materials should be addressed to Osman A. Basaran (e-mail: obasaran@purdue.edu).

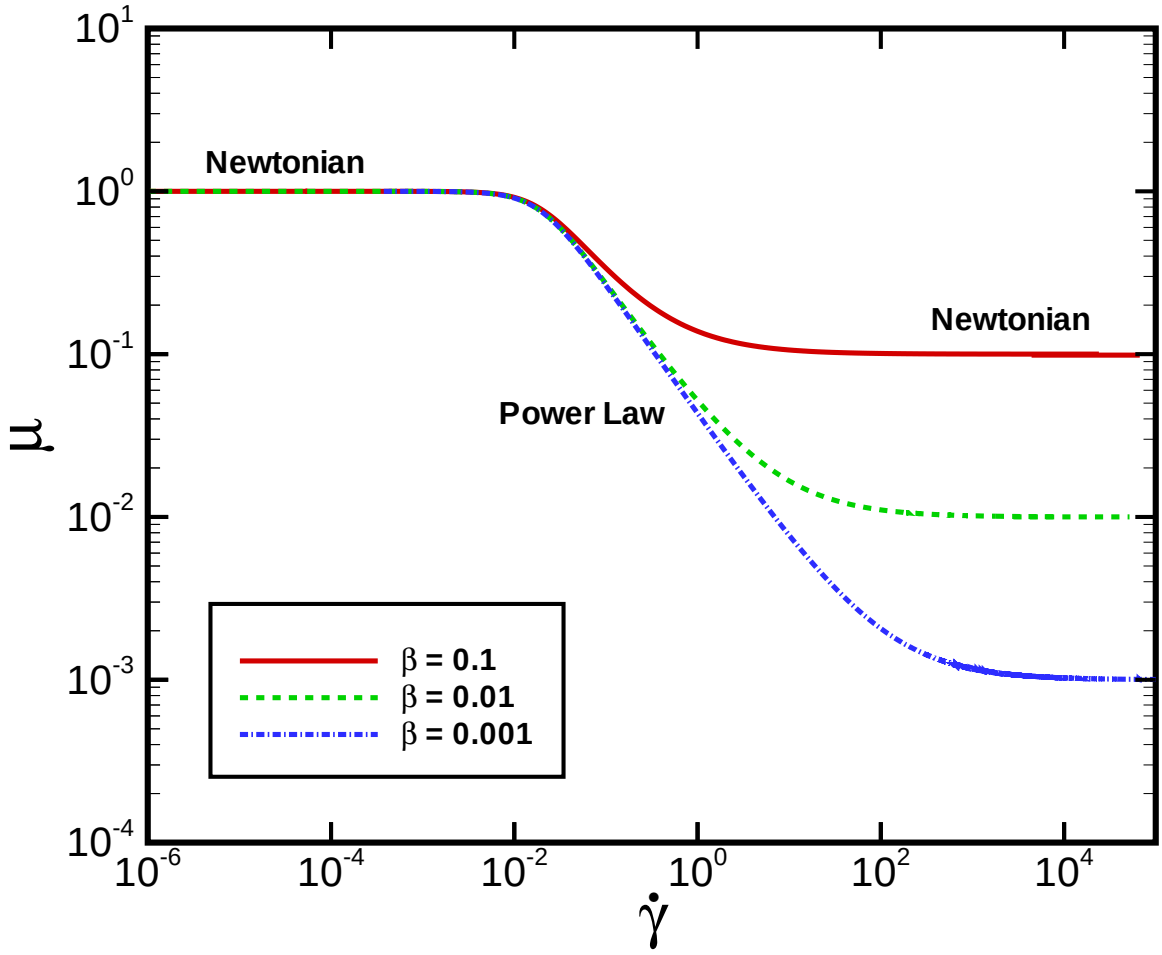

Figure 1: Variation of the dimensionless viscosity $\mu \equiv \tilde{\mu}/\tilde{\mu_o}$ with the dimensionless deformation rate $\dot{\gamma} \equiv \tilde{\alpha}\tilde{\dot{\gamma}}$ for the Carreau model. Here $n = 0.2$.

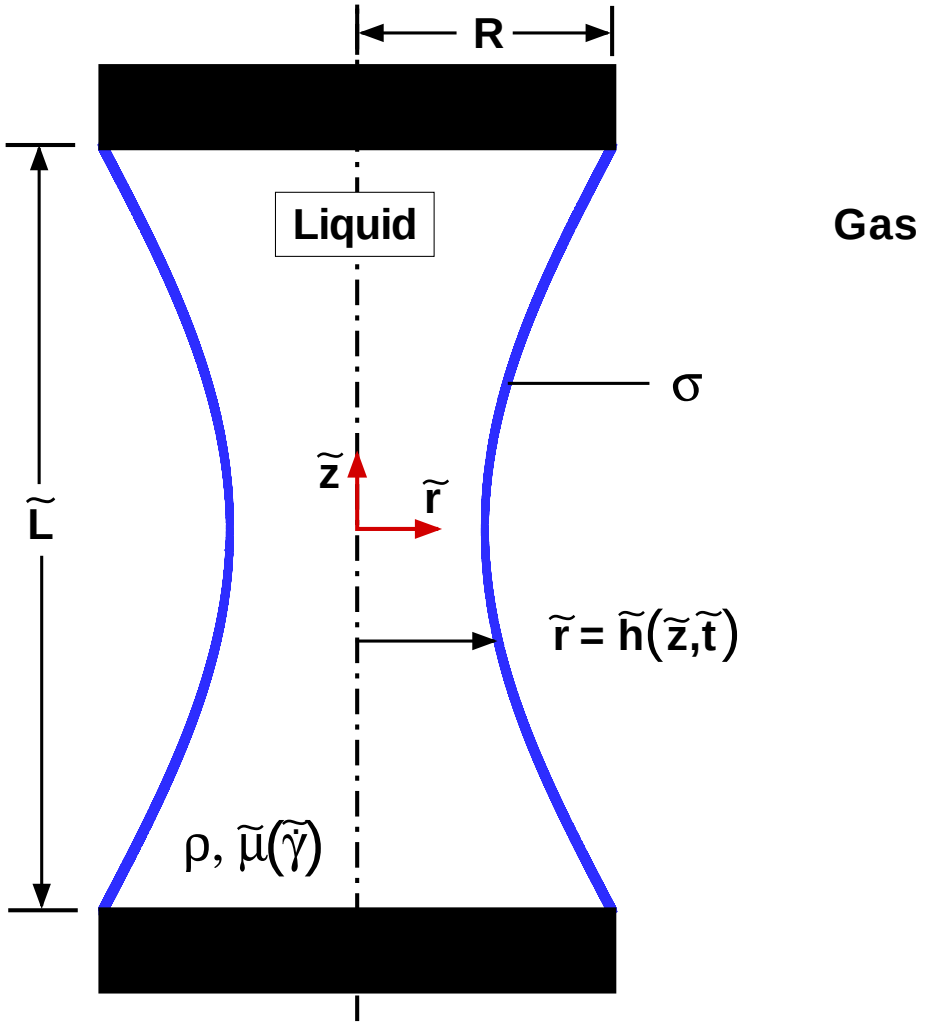

Figure 2: Schematic of a liquid bridge of length $\tilde{L}$ held captive between two disks of equal radii R.

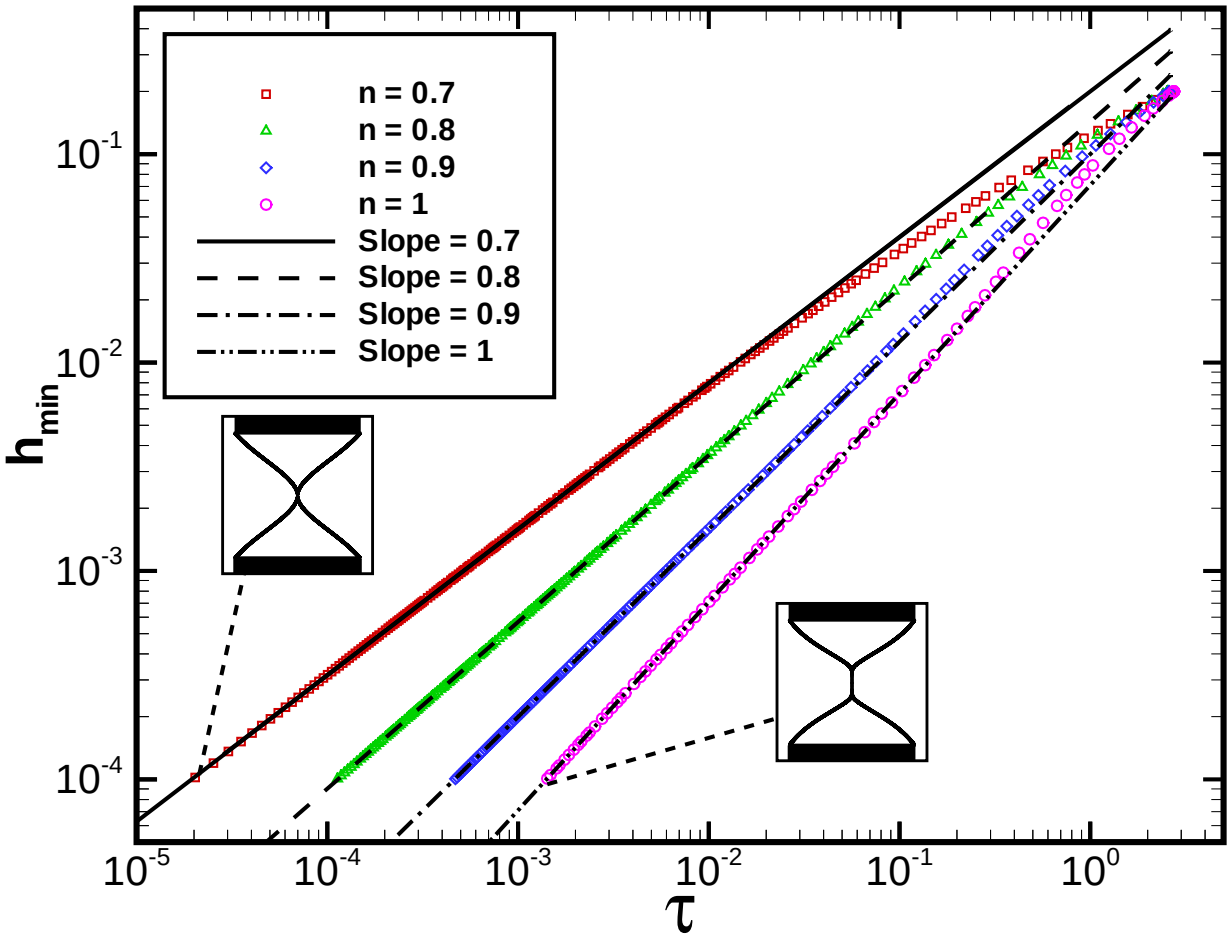

Figure 3: Variation of the computed minimum bridge radius h_{min} with time to breakup τ: radial scaling behavior for bridges of power law fluids of high viscosity with power law exponents $0.7 \leq n \leq 1$ under creeping flow conditions. Here $a = 0.5, Oh^{-1} = 0$, and $\alpha = 1$. The data points shown correspond to computational results obtained with the 1-D code. The straight lines are analytical results from VP scaling theory. The shape insets shown are the bridge shapes at the incipience of breakup, $h_{min} = 1 \times 10^{-4}$, for $n = 0.7$ and 1.

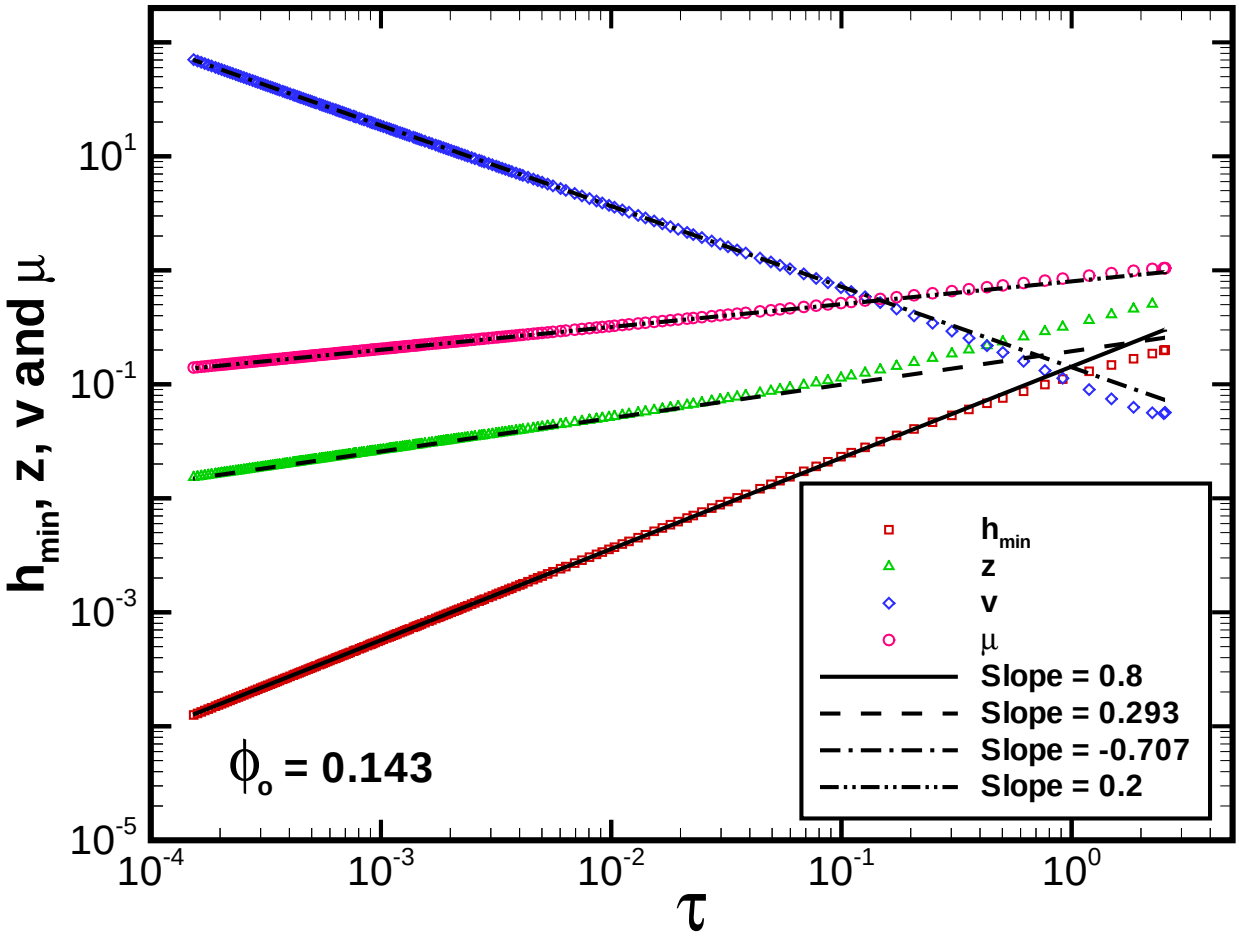

Figure 4: Variation of the computed minimum bridge radius h_{min}, axial distance from the breakup singularity $z \equiv z_{2h_{min}} - z_o$, where $z_{2h_{min}}$ is the axial location where $h = 2h_{min}$, axial velocity $v = v_{2h_{min}}$, and local viscosity at the pinch point $\mu = \mu_{h_{min}}$ with time to breakup τ: radial, axial, axial velocity, and viscosity scalings for a bridge of a power law fluid with $n = 0.8$ under creeping flow conditions. Here $a = 0.5, Oh^{-1} = 0$, and $\alpha = 1$. The data points shown correspond to computational results obtained with the 1-D code. The straight lines are analytical results from VP scaling theory.

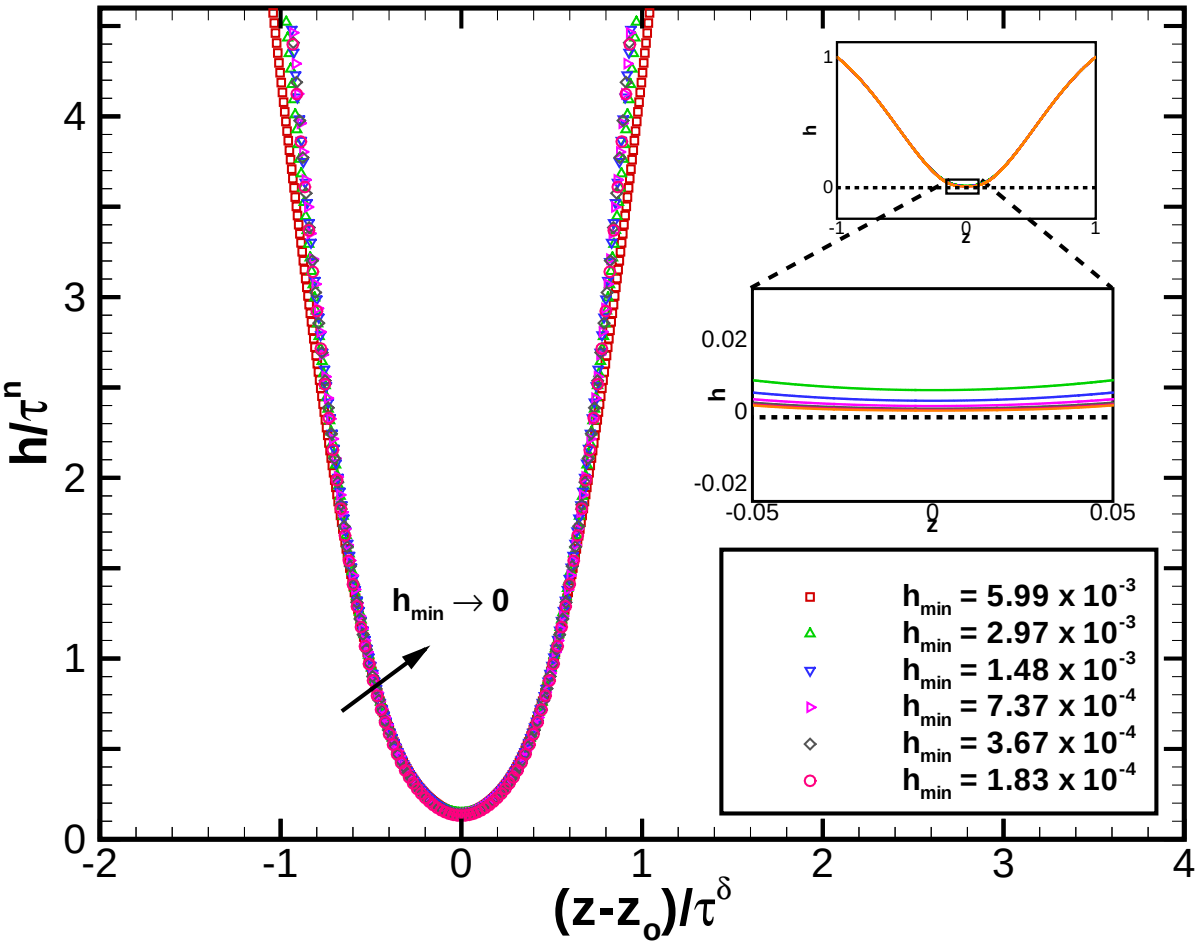

Figure 5: Variation with time of the numerically computed local shape h with axial coordinate measured from the pinch-point $z - z_o$ where both have been rescaled according to radial and axial scalings appropriate to VP scaling theory: self-similarity of local shapes for a power law fluid with $n = 0.8$ under creeping flow conditions. Here $a = 0.5, Oh^{-1} = 0$, and $\alpha = 1$. The data points shown correspond to computational results obtained with the 1-D code. The top inset shows the global bridge shapes and the bottom inset shows local shapes in the vicinity of the pinch point at the incipience of breakup computed with the 1-D code.

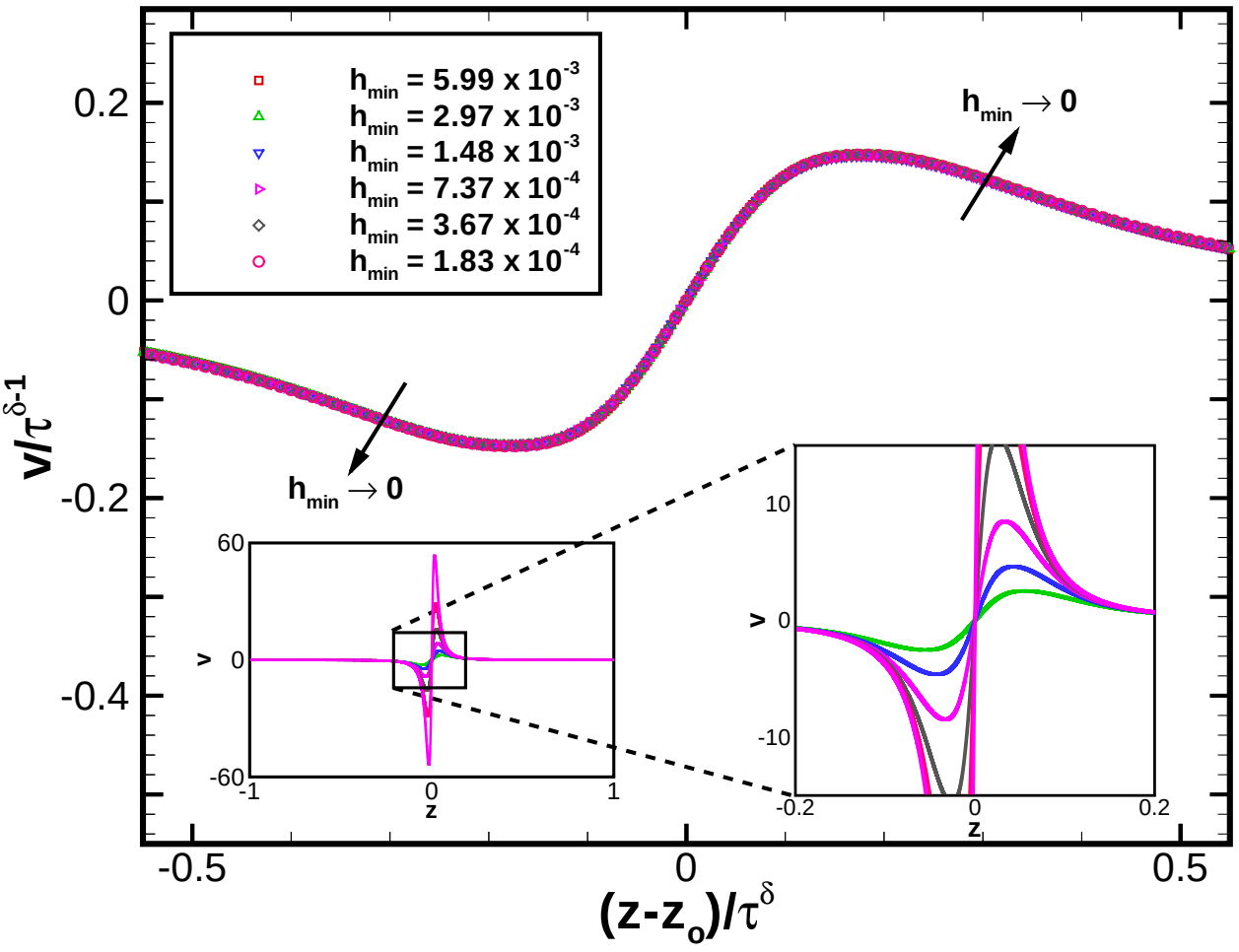

Figure 6: Variation with time of the numerically computed local velocity field v with axial coordinate measured from the pinch-point $z - z_o$ where both have been rescaled according to velocity and axial scalings appropriate to VP scaling theory: self-similarity of local velocity for a power law fluid with $n = 0.8$ under creeping flow conditions. Here $a = 0.5, Oh^{-1} = 0$, and $\alpha = 1$. The data points shown correspond to computational results obtained with the 1-D code. The left inset shows the evolution in time of the axial velocity globally and the right inset shows that in the pinch region computed with the 1-D code.

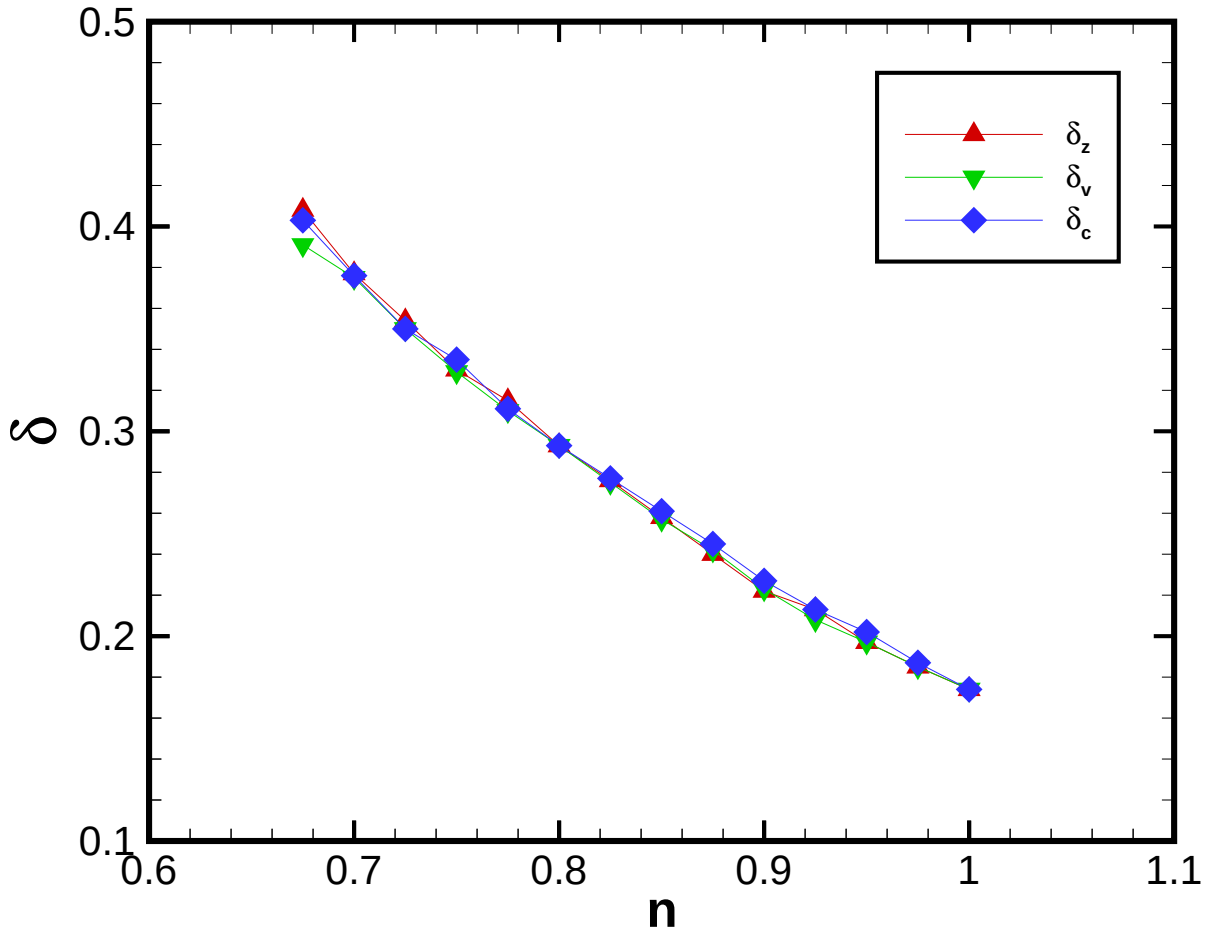

Figure 7: Variation of axial scaling exponent δ with power law exponent n. δ_z is calculated from axial scaling, δ_v is calculated from axial velocity scaling, and δ_c is calculated using the expression given by eq. (28). Here $a = 0.5, Oh^{-1} = 0$, and $\alpha = 1$. All the data points shown have been obtained with the 1-D code.

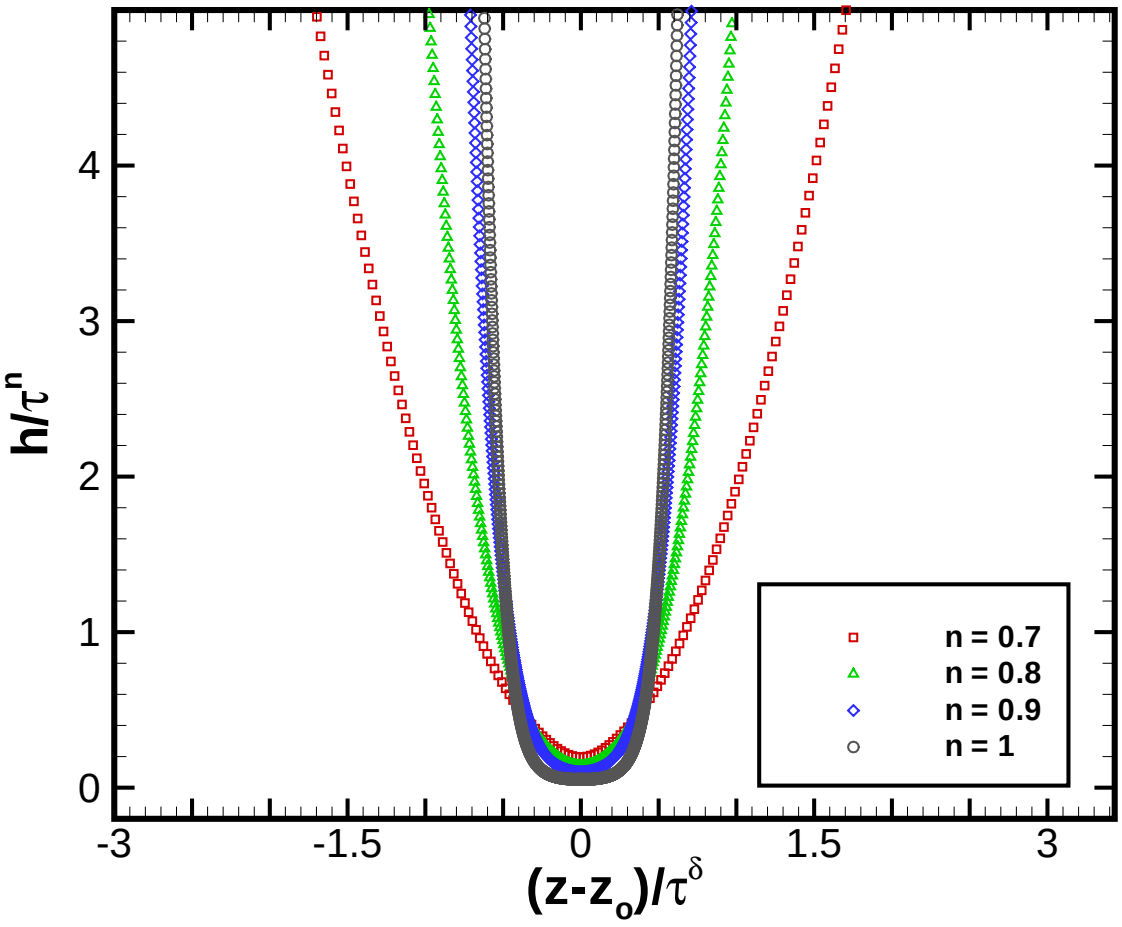

Figure 8: Numerically computed scaling function $\phi(\xi)$ for pinching bridges of power law fluids with $n = 0.7 - 1$ under creeping flow conditions. Here $a = 0.5, Oh^{-1} = 0$, and $\alpha = 1$. The data points shown have been obtained with the 1-D code.

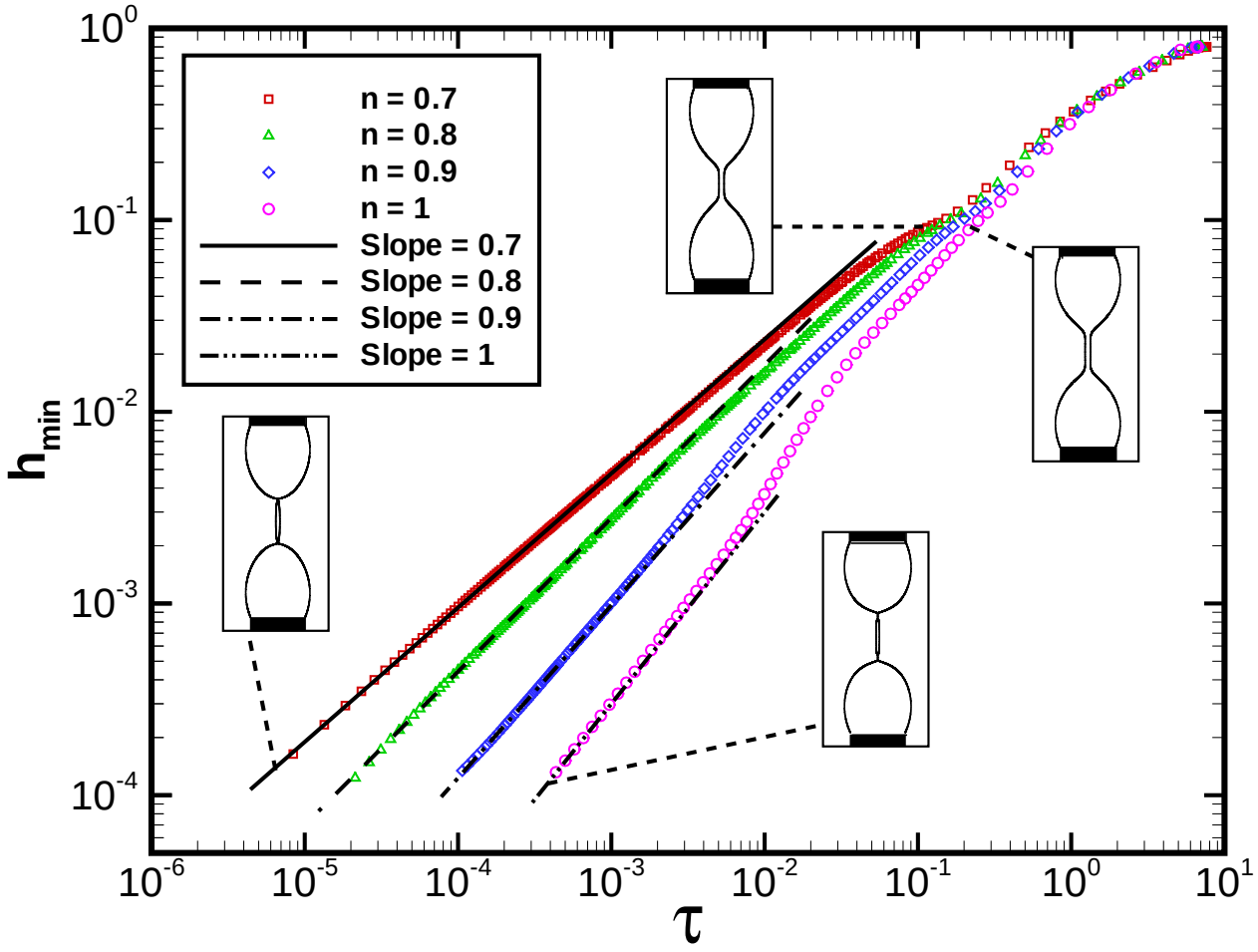

Figure 9: Variation of the computed minimum bridge radius h_{min} with time to breakup τ: radial scaling behavior for bridges of power law fluids of low viscosity with power law exponents $0.7 \leq n \leq 1$. Here $a = 0.2, Oh = 0.1$, and $\alpha = 1$. The data points shown have been obtained with the 1-D code. The straight lines are the analytical results from IVP scaling theory. The shape insets shown are the shapes of two bridges, one with $n = 1$ and the other with $n = 0.7$, at two different stages of their evolution when $h_{min} = 1 \times 10^{-1}$ and 1×10^{-4}.

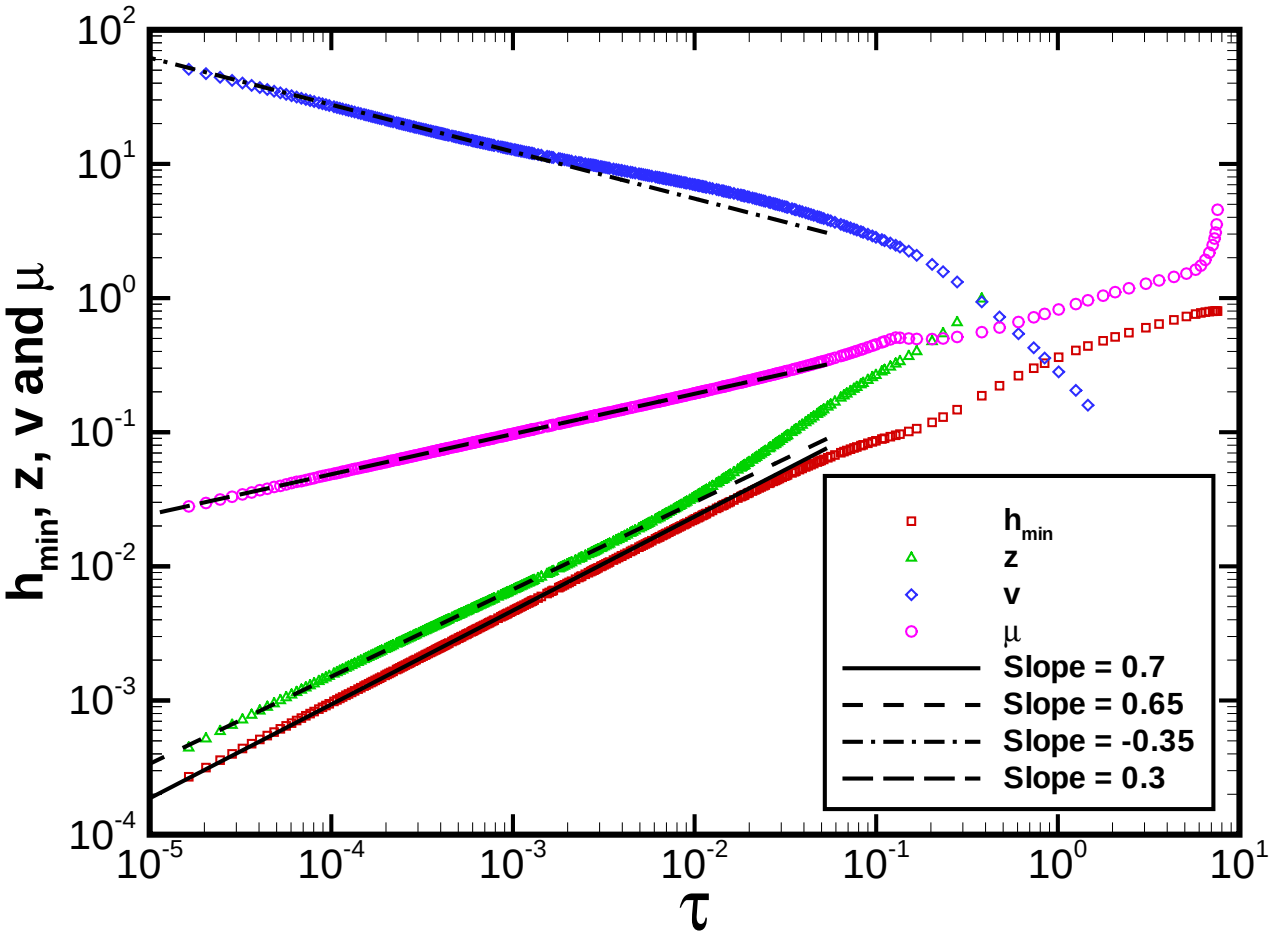

Figure 10: Variation of the computed minimum bridge radius h_{min}, axial distance from the breakup singularity $z \equiv z_{2h_{min}} - z_o$, axial velocity $v \equiv v_{2h_{min}}$, and local viscosity $\mu \equiv \mu_{h_{min}}$ with time to breakup τ: radial, axial, velocity, and viscosity scalings for a bridge of a power law fluid of low viscosity with $n = 0.7$. Here $a = 0.2, Oh = 0.1$, and $\alpha = 1$. The data points shown have been obtained with the 1-D code. The straight lines are the analytical results from IVP scaling theory.

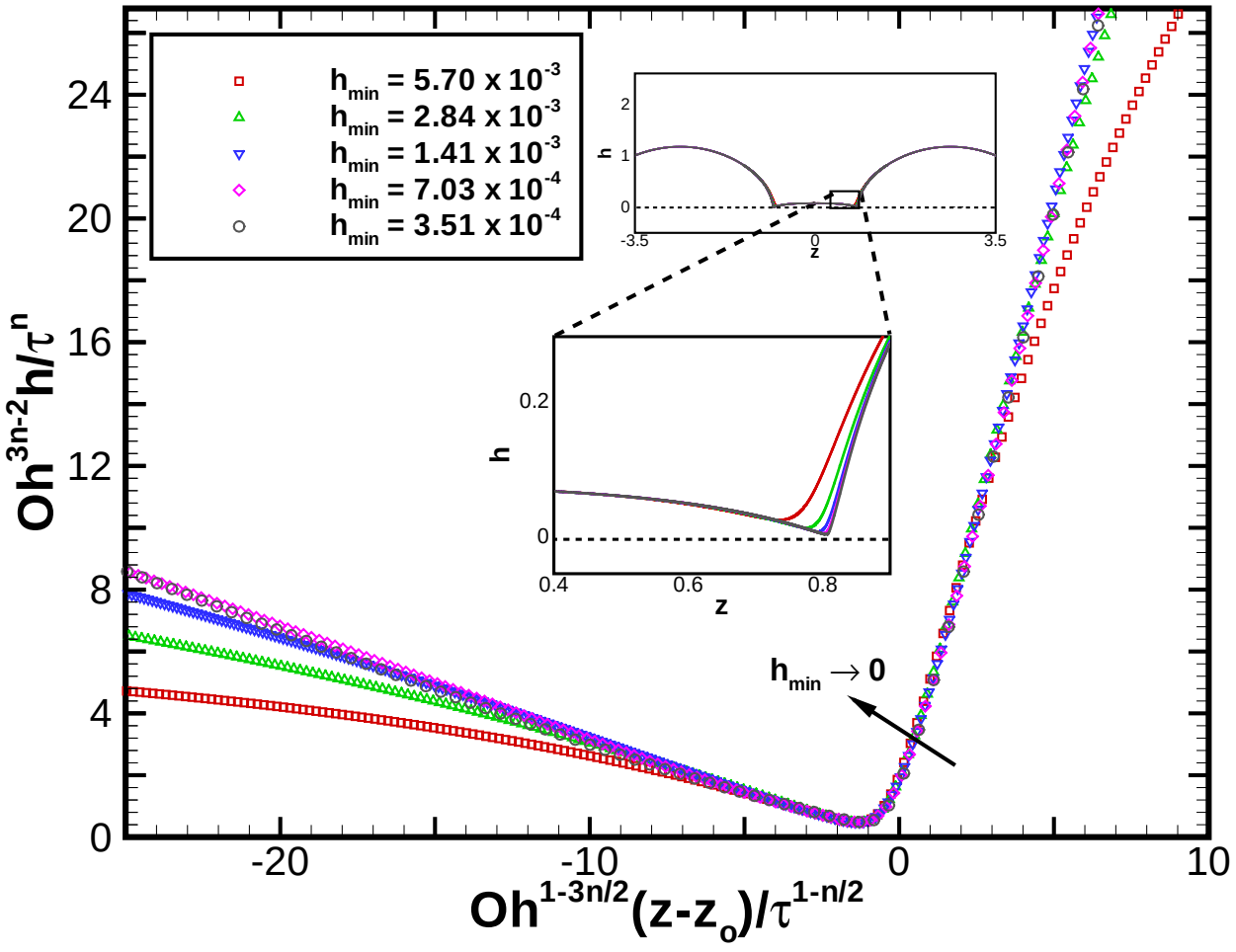

Figure 11: Variation with time of the numerically computed local shapes h with axial coordinate measured from the pinch-point $z - z_o$ where both have been rescaled according to radial and axial scalings appropriate to IVP scaling theory: self-similarity of local shapes for a power law fluid of low viscosity with $n = 0.7$. Here $a = 0.2, Oh = 0.1$, and $\alpha = 1$. The top inset shows global bridge shapes and the bottom inset shows local shapes in the vicinity of the pinch-point at the incipience of breakup computed with the 1-D code.

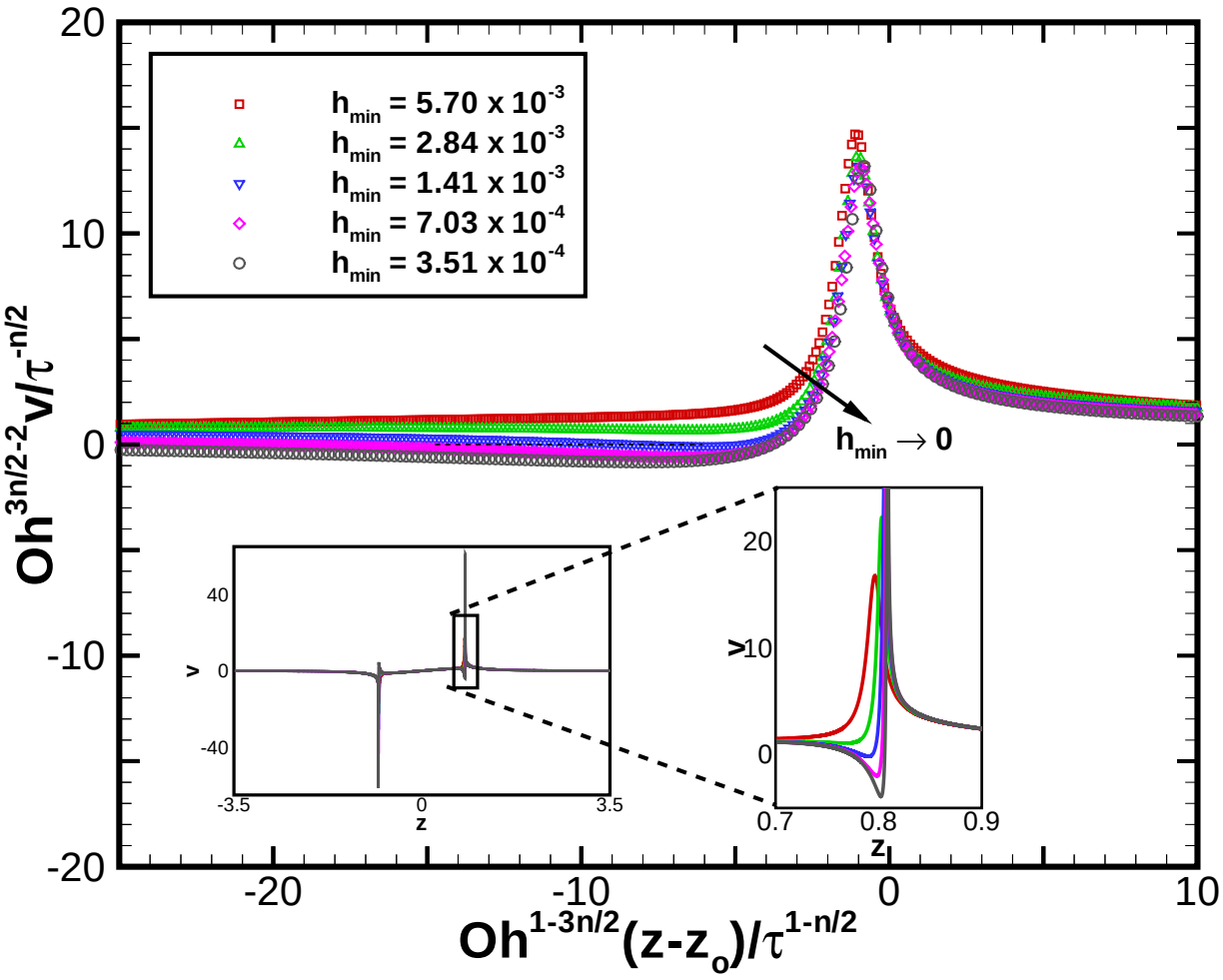

Figure 12: Variation with time of the numerically computed local velocity field v with axial coordinate measured from the pinch-point $z - z_o$ where both have been rescaled according to velocity and axial scalings appropriate to IVP scaling theory: self-similarity of local velocity for a power law fluid of low viscosity with $n = 0.7$. Here $a = 0.2, Oh = 0.1$, and $\alpha = 1$. The left inset shows the evolution in time of the axial velocity globally and the right inset shows that in the pinch region at the incipience of breakup computed with the 1-D code.

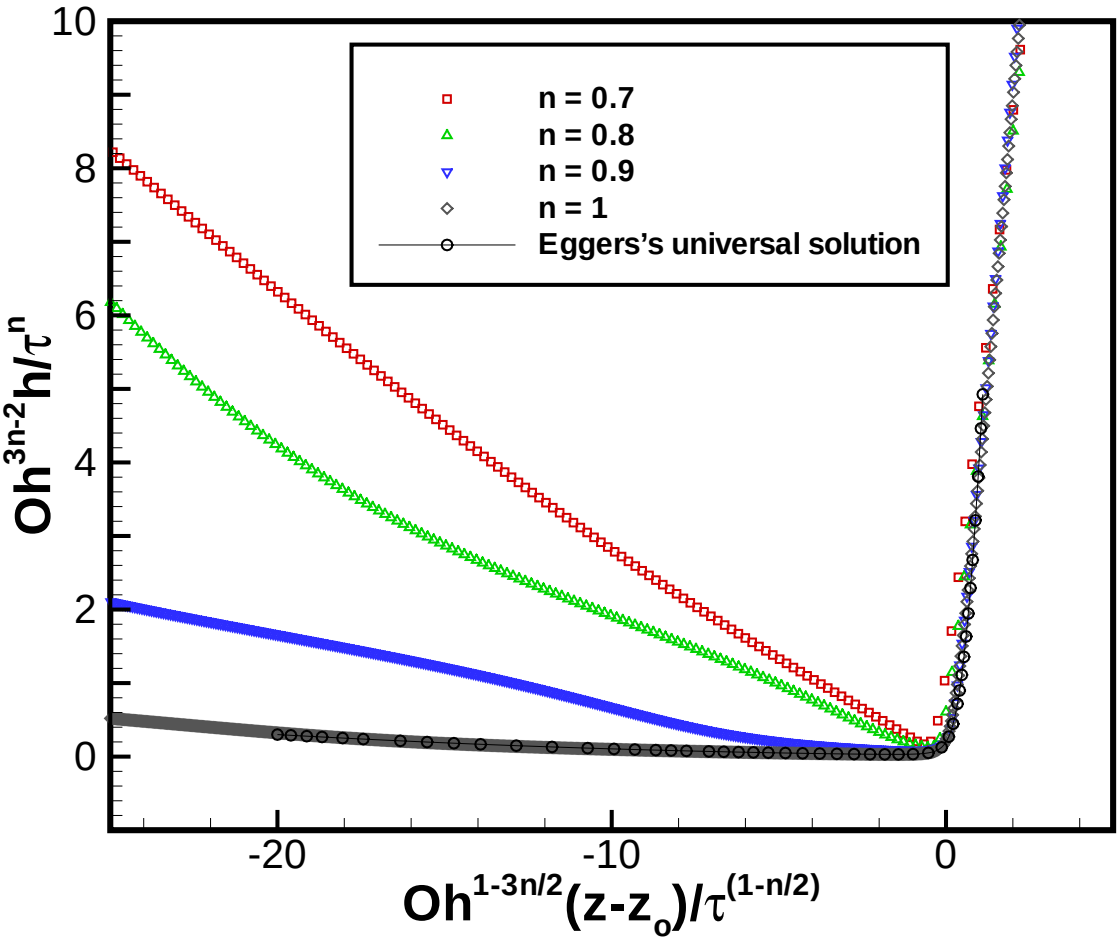

Figure 13: Numerically computed scaling function $\phi(\xi)$ for pinching bridges of power law fluids of low viscosity with $n = 0.7 - 1$. Here $a = 0.2, Oh = 0.1$, and $\alpha = 1$. The data points shown have been obtained with the 1-D code.

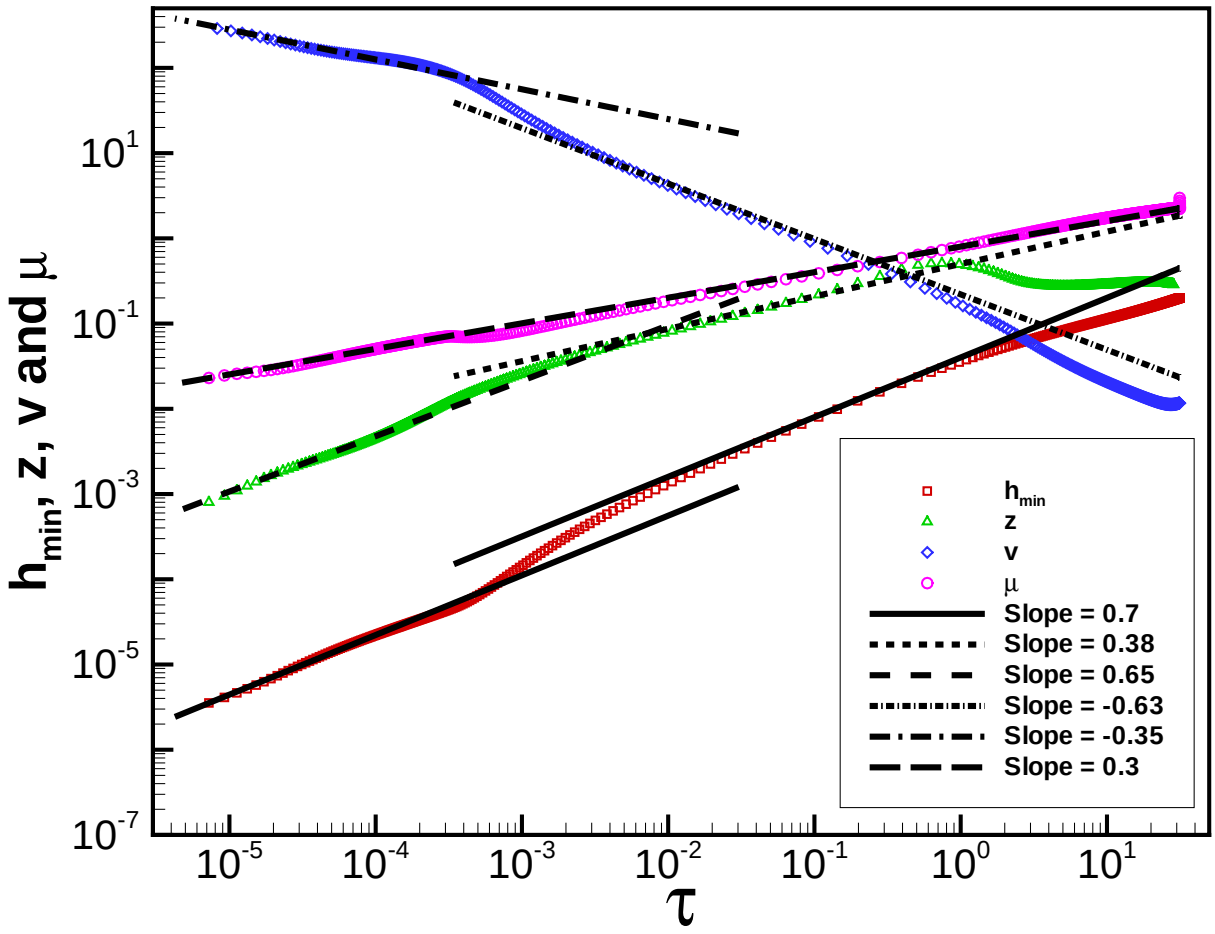

Figure 14: Variation of the computed minimum bridge radius h_{min}, axial distance from the breakup singularity $z \equiv z_{2h_{min}} - z_o$, axial velocity $v \equiv v_{2h_{min}}$, and local viscosity $\mu \equiv \mu_{h_{min}}$ with time to breakup τ: change in scaling from the VP regime to IVP regime. Here $a = 0.2, Oh = 5$, and $\alpha = 1$. The data points shown have been obtained with the 1-D code. The straight lines are the analytical results from VP and IVP scaling theories.

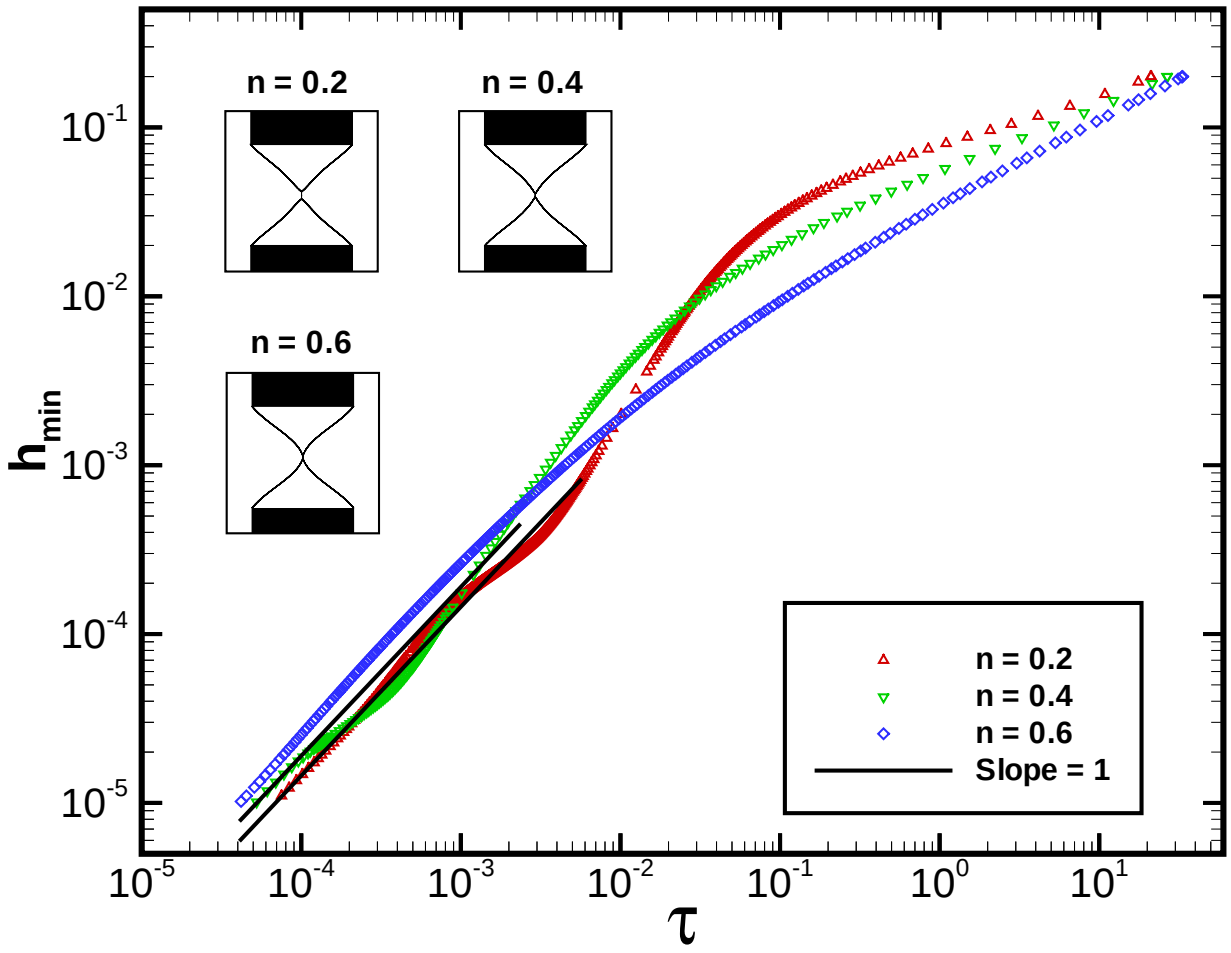

Figure 15: Variation of the computed minimum bridge radius h_{min} with time to breakup τ: radial scaling behavior for bridges of Carreau fluids of high viscosity with exponents $n = 0.2, 0.4$, and 0.6. Here $Oh = 20, a = 0.5, \alpha = 30$, and $\beta = 0.01$. The data points shown have been obtained with the 1-D code. The straight lines are the analytical results from IVP scaling theory. The data show change in scaling from initial power law to final Newtonian scaling. The shape insets show bridge shapes at the incipience of breakup when $h_{min} = 1 \times 10^{-5}$.

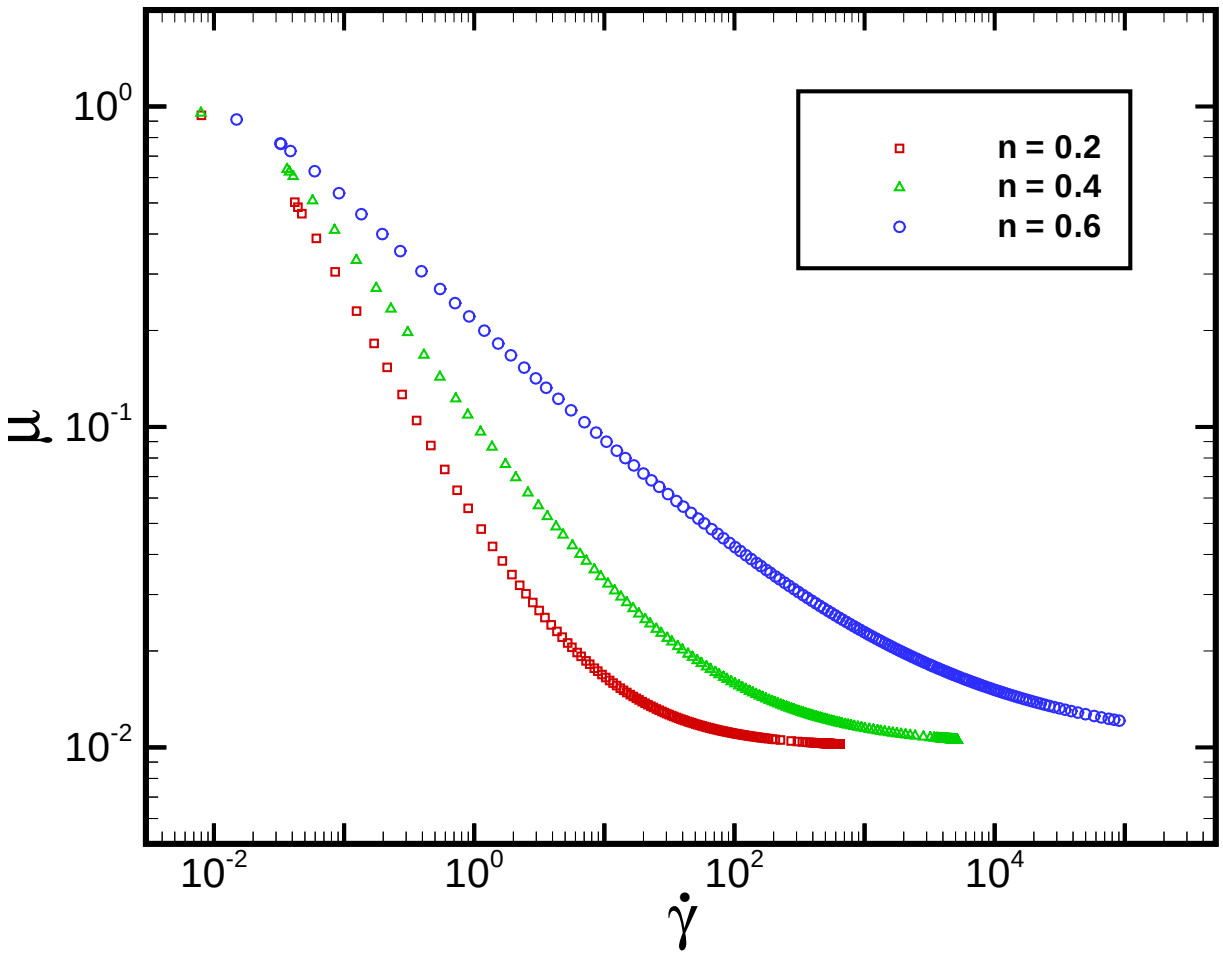

Figure 16: Variation of the computed local viscosity μ at $z = z_{h_{min}}$ with local deformation rate $\dot{\gamma}$ for bridges of Carreau fluids of high viscosity of different n. Here $Oh = 20, a = 0.5, \alpha = 30$, and $\beta = 0.01$. The data points shown have been obtained with the 1-D code.

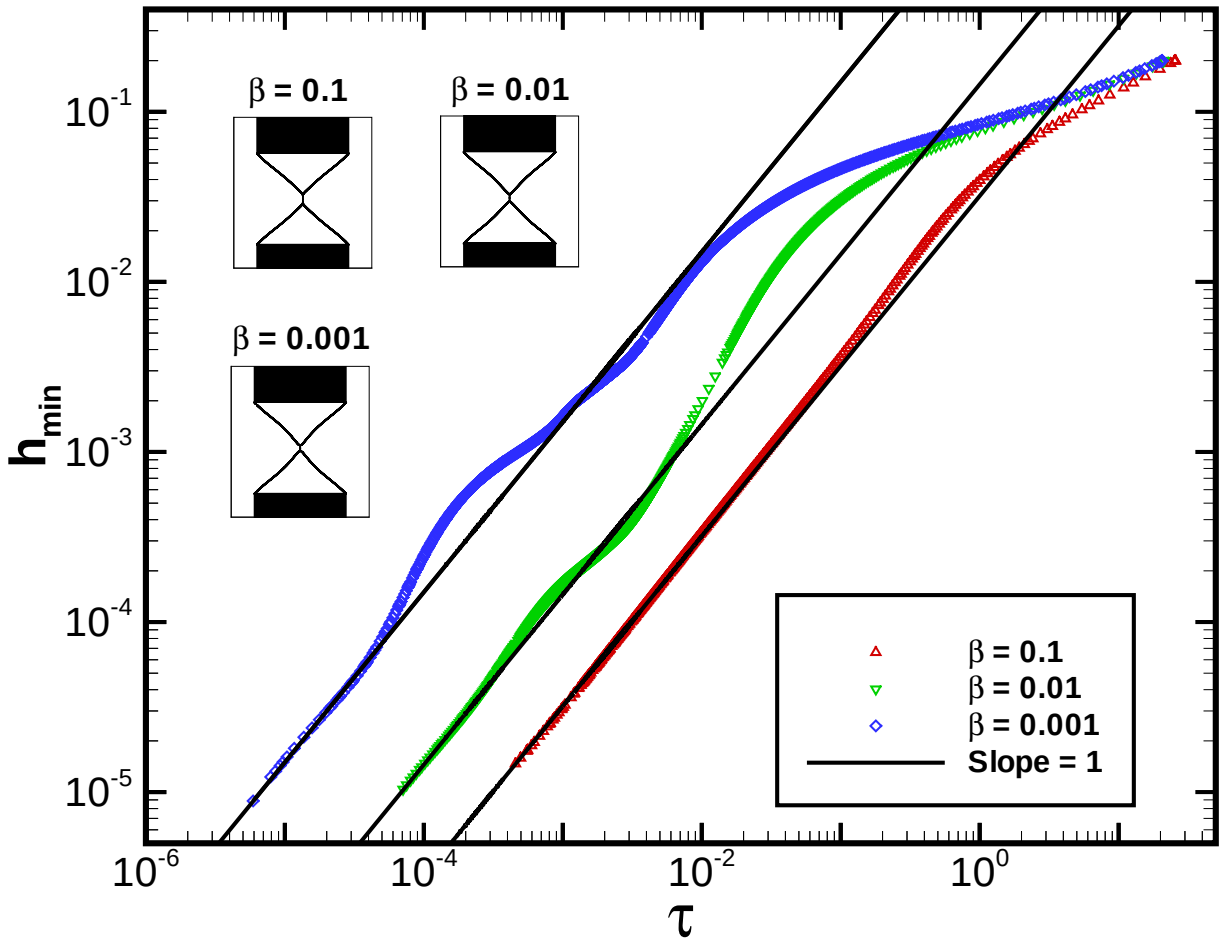

Figure 17: Variation of the computed minimum bridge radius h_{min} with time to breakup τ: radial scaling behavior for bridges of Carreau fluids of high viscosity of different β. Here $Oh = 20, a = 0.5, \alpha = 30$, and $n = 0.2$. The data points shown have been obtained with the 1-D code. The data show a shift in transition points for change in scaling from initial power law to final Newtonian scaling. The shape insets show bridge shapes at the incipience of breakup when $h_{min} = 1 \times 10^{-5}$.

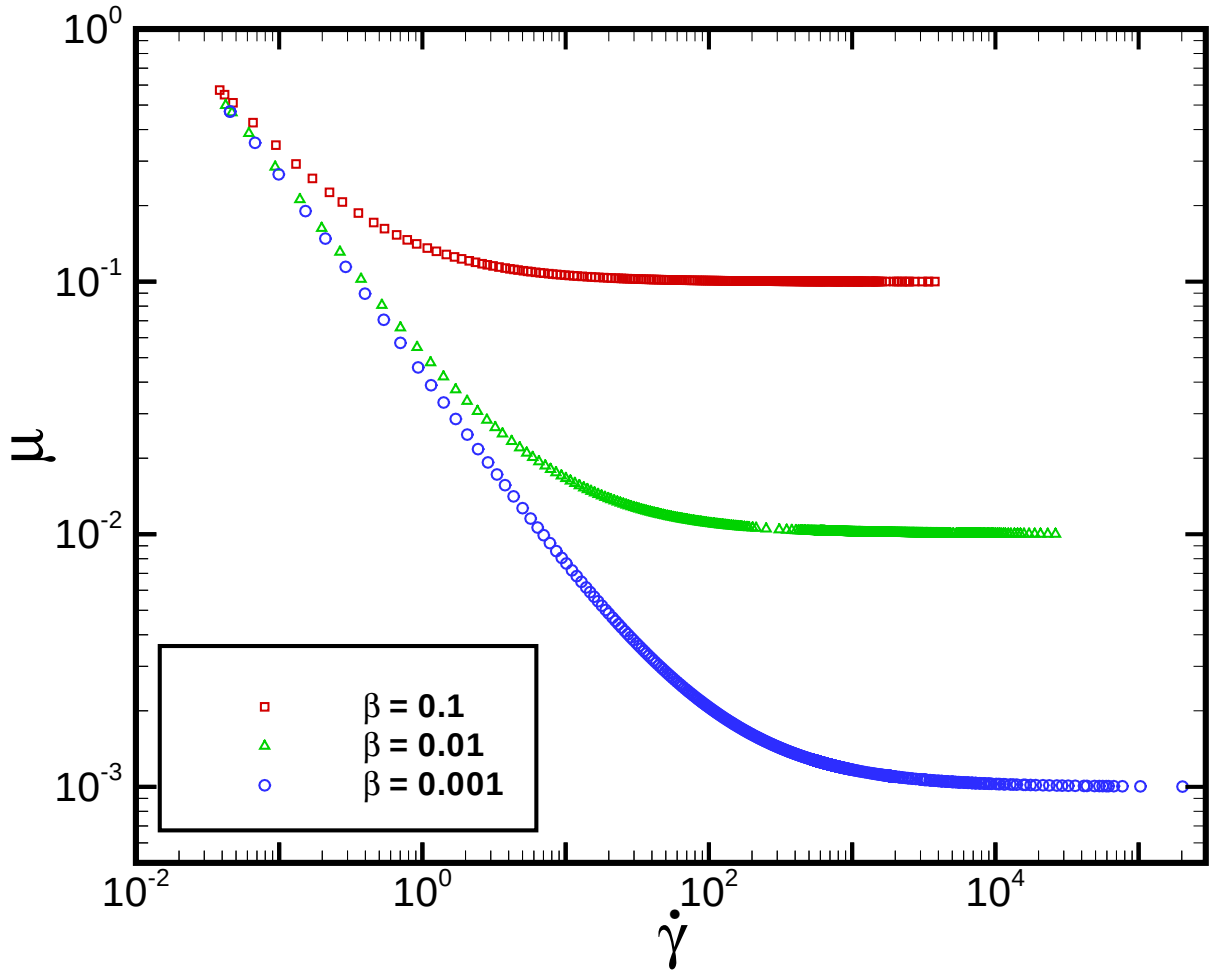

Figure 18: Variation of the computed local viscosity μ at $z = z_{h_{min}}$ with local deformation rate $\dot{\gamma}$ for bridges of Carreau fluids of high viscosity of different β. Here $Oh = 20, a = 0.5, \alpha = 30$, and $n = 0.2$. The data points shown have been obtained with the 1-D code.

Table 1: Variation of numerically computed prefactor ϕ_0 with power law exponent n.

Power law exponent (n)	Prefactor (ϕ_0)
0.675	0.2160
0.700	0.2000
0.725	0.1850
0.750	0.1690
0.775	0.1560
0.800	0.1430
0.825	0.1310
0.850	0.1200
0.875	0.1100
0.900	0.1010
0.925	0.0925
0.950	0.0845
0.975	0.0775
1	0.0709

Table 2: Comparison of the value of the axial scaling exponent calculated by numerical computations, δ, with that calculated using a Taylor series expansion, δ_e, for different values of the power law exponent n.

Power law exponent (n)	δ	δ_e
0.825	0.277	0.298
0.850	0.261	0.272
0.875	0.245	0.251
0.900	0.227	0.234
0.925	0.213	0.218
0.950	0.202	0.205
0.975	0.187	0.190
1	0.175	0.175

Table 3: Variation with the Carreau model exponent n of the values of the rate of deformation and the time remaining to breakup for transition from the power law regime to the Newtonian regime. Here $Oh = 20, \beta = 0.01$, and $\alpha = 30$.

n	$\dot{\gamma}_{transition} = \frac{\beta^{1/(n-1)}}{\alpha}$	$\dot{\gamma}_{transition}$(computed)	$\tau_{transition} = \frac{\alpha}{\beta^{1/(n-1)}}$	$\tau_{transition}$(computed)
0.2	10.5	$\mathcal{O}(10^1)$	0.1	$\mathcal{O}(10^{-1})$
0.4	71.8	$\mathcal{O}(10^2)$	0.014	$\mathcal{O}(10^{-2})$
0.6	3.3×10^3	$\mathcal{O}(10^4)$	3×10^{-4}	$\mathcal{O}(10^{-3})$

Table 4: Variation with the Carreau model parameter β of the values of the rate of deformation and the time remaining to breakup for transition from the power law regime to the Newtonian regime. Here $Oh = 20, n = 0.2$, and $\alpha = 30$.

β	$\dot{\gamma}_{transition} = \frac{\beta^{1/(n-1)}}{\alpha}$	$\dot{\gamma}_{transition}$(computed)	$\tau_{transition} = \frac{\alpha}{\beta^{1/(n-1)}}$	$\tau_{transition}$(computed)
0.1	0.59	$\mathcal{O}(10^0)$	1.7	$\mathcal{O}(10^0)$
0.01	10.54	$\mathcal{O}(10^1)$	0.09	$\mathcal{O}(10^{-1})$
0.001	187.45	$\mathcal{O}(10^2)$	5.3×10^{-3}	$\mathcal{O}(10^{-2})$